A&A 604, A128 (2017)
DOI: 10.1051/0004-6361/201730477

Astronomy & Astrophysics

The *Gaia*-ESO Survey: Galactic evolution of sulphur and zinc[⋆,⋆⋆]

S. Duffau[1,2,3], E. Caffau[4], L. Sbordone[5,1,2], P. Bonifacio[4], S. Andrievsky[6,4], S. Korotin[6,7], C. Babusiaux[4], S. Salvadori[4], L. Monaco[3], P. François[4,8], Á. Skúladóttir[9,10], A. Bragaglia[11], P. Donati[11,12], L. Spina[13], A. J. Gallagher[4], H.-G. Ludwig[14,4], N. Christlieb[14], C. J. Hansen[15,16], A. Mott[17], M. Steffen[17], S. Zaggia[18], S. Blanco-Cuaresma[19], F. Calura[11], E. Friel[20], F. M. Jiménez-Esteban[21], A. Koch[22], L. Magrini[23], E. Pancino[23,24], B. Tang[25], G. Tautvaišienė[26], A. Vallenari[18], K. Hawkins[27] G. Gilmore[28], S. Randich[23], S. Feltzing[29], T. Bensby[29] E. Flaccomio[34], R. Smiljanic[30], A. Bayo[31], G. Carraro[32], A. R. Casey[28], M. T. Costado[33], F. Damiani[34], E. Franciosini[23], A. Hourihane[28], P. Jofré[28,35], C. Lardo[36], J. Lewis[28], L. Morbidelli[23], S. G. Sousa[37], and C. C. Worley[28]

(Affiliations can be found after the references)

Received 20 January 2017 / Accepted 10 April 2017

ABSTRACT

Context. Due to their volatile nature, when sulphur and zinc are observed in external galaxies, their determined abundances represent the gas-phase abundances in the interstellar medium. This implies that they can be used as tracers of the chemical enrichment of matter in the Universe at high redshift. Comparable observations in stars are more difficult and, until recently, plagued by small number statistics.
Aims. We wish to exploit the *Gaia*-ESO Survey (GES) data to study the behaviour of sulphur and zinc abundances of a large number of Galactic stars, in a homogeneous way.
Methods. By using the UVES spectra of the GES sample, we are able to assemble a sample of 1301 Galactic stars, including stars in open and globular clusters in which both sulphur and zinc were measured.
Results. We confirm the results from the literature that sulphur behaves as an α-element. We find a large scatter in [Zn/Fe] ratios among giant stars around solar metallicity. The lower ratios are observed in giant stars at Galactocentric distances less than 7.5 kpc. No such effect is observed among dwarf stars, since they do not extend to that radius.
Conclusions. Given the sample selection, giants and dwarfs are observed at different Galactic locations, and it is plausible, and compatible with simple calculations, that Zn-poor giants trace a younger population more polluted by SN Ia yields. It is necessary to extend observations in order to observe both giants and dwarfs at the same Galactic location. Further theoretical work on the evolution of zinc is also necessary.

Key words. Galaxy: abundances – Galaxy: evolution – Galaxy: disk – stars: abundances – open clusters and associations: general – globular clusters: general

1. Introduction

It is known from observations of the Galaxy's interstellar medium (ISM) that many chemical elements in the gas phase can be depleted into dust grains (such elements are also referred to as refractory). Zinc and sulphur are two of the few elements that are relatively unaffected by this in the ISM (i.e. volatile, see e.g. Savage & Sembach 1996). This makes sulphur and zinc interesting elements to investigate, and for this reason we make use of the large sample of stars observed by the *Gaia*-ESO Survey (GES, Gilmore et al. 2012; Randich et al. 2013), for which both sulphur and zinc have been analysed, to investigate the abundances of these relatively volatile elements in Galactic stars and to exploit their potential as tracers of Galactic chemical evolution.

Sulphur. Sulphur is produced in the final stage of the evolution of massive stars, type II supernovae (SNe, Woosley & Weaver 1995; Limongi & Chieffi 2003; Chieffi & Limongi 2004, typically on timescales of less than 30 Myr). On the other hand, although the elements of the iron-peak are produced by type II SNe, they are mainly produced in type Ia SNe (SN Ia), which produce little to no α-elements (Nomoto et al. 1984; Iwamoto et al. 1999). To picture the evolution of the stellar populations in a galaxy it is important to derive the chemical abundances of both the α-elements and iron-peak elements. In fact, abundance ratios between elements formed on different timescales, such as [α/Fe], can be used as cosmic clocks, and allow us to clarify the star formation history of our targets. The first phases of evolution of a galaxy are characterised by a low content of metals, because only a small number of massive stars have had enough time to evolve and explode and/or transfer mass to a companion which can in turn reach the mass limit and explode. In both cases, they enrich the environment with the metals synthesised during their stellar life. This early environment is mainly characterised by enrichment from type II SNe but there is hardly any contribution from type Ia SNe, possibly with little traces of the products of the promptest type Ia explosions at evolutionary times greater than 30−40 Myr (see Mannucci et al. 2006; Greggio & Renzini 1983). The metal-poor environment is then characterised by an over abundance of α-elements with respect to iron-peak elements when compared to the Sun. This is usually referred to as the α-elements enhancement, generally observed in metal-poor stars (e.g. Venn et al. 2004; Cayrel et al. 2004; Bonifacio et al. 2009; Hayden et al. 2015) and also theoretically predicted (Tinsley 1979; Matteucci & Brocato 1990).

⋆ Based on observations collected at the European Organisation for Astronomical Research in the Southern Hemisphere under ESO programmes 188.B-3002, 193.B-0936.
⋆⋆ The full table of S abundances is only available at the CDS via anonymous ftp to cdsarc.u-strasbg.fr (130.79.128.5) or via http://cdsarc.u-strasbg.fr/viz-bin/qcat?J/A+A/604/A128

At the solar metallicity regime, on the other hand, the ratio of α-elements over iron is the same as in the Sun, because type Ia SNe have had time to explode and enrich the ISM with iron-peak elements.

A few S I features are detected as absorption lines in the spectra of late-type stars. Sulphur lines typically used to derive the sulphur abundance belong to five S I multiplets (Mult.)[1]. Mult. 1 at 920 nm, Mult. 3 at 1045 nm, Mult. 6 at 869 nm, Mult. 8 at 670 nm and Mult. 10 at 605 nm. A forbidden line at 1082 nm can only be used to analyse giant stars. This line has an equivalent width of about 0.2 pm in the solar spectrum (Caffau & Ludwig 2007) therefore it can be used to derive $A(S)$[2] in dwarf stars at metal-rich regime in extremely high quality spectra only. Two decades after the pioneering investigation of sulphur by Wallerstein & Conti (1964), who analysed nine stars in six globular clusters, the systematic analysis of sulphur established itself (François 1987, 1988).

Sulphur, as an α-element, is expected to scale with iron in solar metallicity stars ([S/Fe][3] $\approx$ 0.0), to increase with respect to iron ([S/Fe] $>$ 0.0) as metallicity decreases in the range of $-1.0 <$ [Fe/H] < -0.3, and to have a quite constant positive value of about [S/Fe] $\approx +0.4$ in the metal-poor regime [Fe/H] < -1.0. In the theoretical framework, Chiappini et al. (1999) and Kobayashi et al. (2006) investigated the Galactic evolution of sulphur by calculating its evolution in the solar neighbourhood, adopting their own nucleosynthesis yields. They obtained their yields based on the new developments at that time in the observational and theoretical studies of SNe and extremely metal-poor stars in the Galactic halo. In Fig. 11 of Kobayashi et al. (2006), an almost flat [S/Fe] is predicted in the range $-3.0 <$ [Fe/H] < -1.0. Unlike other α-elements, like silicon and calcium, sulphur is relatively volatile. This in turn means that it is not locked into dust grains that form in the ISM (but see Calura et al. 2009; Jenkins 2009). As a consequence the sulphur abundance derived in stellar photospheres can be directly compared to the sulphur present in the ISM, for instance derived from emission lines in spectra of Blue Compact Galaxies and from resonance absorption lines in Damped Ly-α systems (Garnett 1989; Centurión et al. 2000).

Although all the recent works agree on an average increase of [S/Fe] below solar metallicity, not all studies agree on a constant [S/Fe] at metal-poor regime. Instead, various scenarios have been reported: a constant increase of [S/Fe] as metallicity decreases (see Israelian & Rebolo 2001; Takada-Hidai et al. 2002); an increase followed by a flat [S/Fe] at the metal-poor regime as metallicity decreases (Nissen et al. 2004, 2007); or a bimodal behaviour of [S/Fe] at the metal-poor regime (Caffau et al. 2005a). Most recent papers tend to agree on a flat [S/Fe] in metal-poor stars (Spite et al. 2011; Matrozis et al. 2013).

After the pioneering work of Caffau et al. (2005b), who investigated sulphur in three stars belonging to Terzan 7, a globular cluster belonging to the Sagittarius dwarf Spheroidal galaxy, sulphur abundance has been derived in several open and globular clusters. Recently Skúladóttir et al. (2015) analysed the S I lines of Mult. 1 in a sample of 85 stars in the Sculptor dwarf spheroidal galaxy, in the metallicity range $-2.5 <$ [Fe/H] < -0.8. They found that sulphur behaves as the other α-elements in Sculptor, when effects due to departures from local thermodynamical equilibrium (LTE) are taken into account.

In Tables 1 and 2 we summarise some important literature results for abundance determination of sulphur in the Galaxy for field stars, stars in open and globular clusters, and stars in some extra-galactic objects as well[4]. The metallicity ranges, as well as the observed trends (flat, sloping etc.), are indicated and comments regarding the data have been added for clarity.

Sulphur has also been derived in the Apache Point Observatory Galactic Evolution Experiment (APOGEE) project. APOGEE is part of the third phase of the Sloan Digital sky survey (SDSS-III). A near-infrared spectrograph (1.51−1.70 μm; R = 22 500) was used to collect spectra for about 150 000 stars over three years (Holtzman et al. 2015). Stellar atmospheric parameters were released, together with abundance data for 15 elements, including sulphur (see Fig. 14 in Holtzman et al. 2015) derived from the S I lines at 1.5 μm. Hayden et al. (2015) selected about 70 000 cool giants from SDSS data release 12 and studied the behaviour of the Milky Way disk in the [α/Fe] versus [Fe/H] plane over a large volume, namely within 2 kpc from the plane, at radial distance $3 \leq R \leq 15$ kpc of the galactic centre (bulge excluded). Together with O, Mg, Si, Ca and Ti, sulphur is one of the elements that are combined to provide the [α/Fe] parameter in APOGEE. Hayden et al. (2015) found that in the inner disk ($R < 5$ kpc), stars are distributed along a single sequence, while in the outer disk ($R > 5$ kpc), stars are distributed along a high and a low α sequence (see their Figs. 3 and 4). Such a double sequence was predicted theoretically by Calura & Menci (2009). Hayden et al. (2015) found the shape of the high α sequence to remain constant with the radial distance, although very few of them were found at $R > 11$ kpc (see also Nidever et al. 2014). The high and low α sequences are indicated to correspond to the thick and thin disk populations (Holtzman et al. 2015).

Some special stars of relevance have also been investigated. Bonifacio et al. (2012), analysing the Mult. 3, could derive only an upper limit for the sulphur content in HE 1327-2326 (one of the most iron-poor stars known Frebel et al. 2005). Roederer et al. (2016) derived the first abundance of sulphur in a carbon-enhanced metal-poor star (below [Fe/H] = −3, but see also Skúladóttir et al. 2015) by analysing BD+44°493. At this iron abundance regime ([Fe/H] = −3.8), the usually investigated S I features are too weak. They investigated three ultraviolet S I lines at 181 nm in a spectrum observed with HST using the Cosmic Origins Spectrograph. They derived [S/Fe] = +0.07 ± 0.41. This value is compatible with the behaviour of [S/Fe] in metal-poor stars, albeit with large uncertainty.

Two independent Non-LTE (NLTE) investigations can be found in Takeda et al. (2005) and Korotin (2008, 2009). They conclude that NLTE effects are usually large for the strong lines of Mult. 1 and 3, while they are much smaller for the weak lines of Mult. 6 and 8.

Zinc. Zinc, also a relatively volatile element, was believed to be an accurate tracer of iron-peak elements, since [Zn/Fe] $\approx$ 0 in early measurements of thin disk stars (e.g. Sneden & Crocker 1988; Sneden et al. 1991). Zinc has thus been historically used to infer the iron content of the gas in damped Lyman-α systems (DLAs, e.g. see Wolfe et al. 2005, for a complete review – in particular their Sect. 3.2). In principle, measurements of [S/Zn] versus [Zn/H] in stellar photospheres can thus be directly compared with the abundances of distant DLAs, which might represent the

[1] We adopt the multiplet numbering of Moore (1945).

[2] $A(X) = \log_{10}\left(\frac{N(X)}{N(H)}\right) + 12$.

[3] $[X/Y] = \log_{10}\left(\frac{N(X)}{N(Y)}\right)_* - \log_{10}\left(\frac{N(X)}{N(Y)}\right)_\odot$.

[4] In listing [Fe/H] and [S/Fe] in these tables we did not attempt to homogenize the respective solar abundance scales, since all the values listed are indicative and would not vary in any significant way.

Table 1. Summary of literature regarding Galactic sulphur abundances.

Reference	Mult. line	N_{obs}	NLTE	Target type	Flat range	Slope range	Comments
Clegg et al. (1981)	6	20	–	F&G MS	–	$-0.9 < [Fe/H] < +0.4$	large scatter
François (1987)	6	13	–	MP dwarfs	$[Fe/H] < -0.5$	$-0.5 < [Fe/H] < +0.3$	1 halo star
François (1988)	6	12	–	field dwarfs	$-1.3 < [Fe/H] < -0.5$	–	5 are halo stars
Takada-Hidai & Takeda (1996)	6	11	√	peculiar stars	solar	–	
Israelian & Rebolo (2001)	6	8	–	MP	–	$-3.0 < [Fe/H] < -0.6$	negligible NLTE
Takada-Hidai et al. (2002)	6	68	√	field stars	–	$-3 < [Fe/H] < 0.0$	
Chen et al. (2002)	6, 8, 10	26	–	disc stars	$-1.0 < [Fe/H] < -0.5$	$-0.5 < [Fe/H] < +0.5$	–
Chen et al. (2003)	6, 8, 10	15	–	old MR	–	$-0.1 < [Fe/H] < +0.5$	–
Ecuvillon et al. (2004)	8	112/31	–	planet/no planet	–	$-0.8 < [Fe/H] < +0.5$	–
Nissen et al. (2004)	1, 8	34	–	dwarf/subgiant halo	$-3.2 < [Fe/H] < -0.8$	–	3D effects small, two deviant stars
Ryde & Lambert (2004)	1	10	–	–	$-3.0 < [Fe/H] < -0.7$	–	–
Korn & Ryde (2005)	1, 6	3	–	MP	$-2.43 < [Fe/H] < -2.08$	–	–
Caffau et al. (2005a)	1, 6, 8	74	–	–	$-3.2 < [Fe/H] < -1.0$ (*)	$-1.0 < [Fe/H] < +0.5$	in combined lit.sample (253 stars) (*) dual behaviour at $[Fe/H] < -1$
Takeda et al. (2005)	1, 3, 6	3	√	FGK Stars	$-3.17 < [Fe/H] < -2.0$ (*)	$-2.0 < [Fe/H] < +0.47$	in combined lit. sample (175 stars) (*) dual behaviour at $[Fe/H] < -2$
Ryde (2006)	[SI]	14	–	disk giants/subgiants	–	$-0.66 < [Fe/H] < +0.03$	–
Nissen et al. (2007)	1, 6	40	√	MS halo	$-3.3 < [Fe/H] < -1.0$	–	low scatter
	3	1	–	–	$[Fe/H] = -1.69$	–	–
Caffau et al. (2007)	3	5	√	F-K MS	–	–	test for Mult.3 analysis, good agreement with Mult. 6 and 8 results
Caffau et al. (2010)	3	4	√	MP halo	–	–	no flat behaviour, scatter in $-2.42 < [Fe/H] < -1.19$
Takeda & Takada-Hidai (2011)	3	33	√	halo/disk	$-2.5 < [Fe/H] < -1.5$	$-1.0 < [Fe/H] < 0.0$	jump in A(S) with [Fe/H] $-3.7 < [Fe/H] < -2.5$
Takeda & Takada-Hidai (2012)	3	13	√	TO dwarfs & giants	$-3.2 < [Fe/H] < -1.9$	–	–
Spite et al. (2011)	1	33	√	EMP	$-3.5 < [Fe/H] < -2.9$	–	–
Jönsson et al. (2011)	3, [SI]	10	√, –	giants	$-3.4 < [Fe/H] < -1.5$	–	A(S) from [SI] larger than from Mult. 3
Matrozis et al. (2013)	[SI]	39	–	MP giants	$-2.3 < [Fe/H] < -1.0$	$-1.0 < [Fe/H] < 0.0$	–
Takeda et al. (2016)	6, 8	239	√	giants	–	$-0.8 < [Fe/H] < +0.2$	high scatter (Mult. 6), A(S) from Mult. 8
	6, 8	160	√	dwarfs	–	$-1.3 < [Fe/H] < +0.5$	A(S) from Mult. 8
Caffau et al. (2016)	3	4	√	dwarfs	–	–	–

Table 2. Summary of literature regarding sulphur abundances in open clusters, globular clusters, and extra-galactic stars.

Reference	Mult. line	N_{obs}	Object	[Fe/H] dex	[S/Fe] dex	Consistent with MW?	Comments
Caffau et al. (2005b)	1	3	Terzan 7 (Sgr dSph)	−0.5	−0.05	–	Lower than MW, consistent with Sgr dSph
Sbordone et al. (2009)	1	4	NGC 6752	−1.43	$\langle[S/Fe]\rangle = +0.49 \pm 0.15$	√	–
	1	9	47 Tuc	−0.67	$\langle[S/Fe]\rangle = +0.18 \pm 0.14$	√	S-Na corr.
Koch & Caffau (2011)	1	1	NGC 6397	−2.1	$\langle[S/Fe]\rangle = +0.52 \pm 0.20$	√	–
Caffau et al. (2014)	1	10	M4	−1.36	0.51	√	–
	1	1	Trumpler 5	−0.53	−0.23	–	low [S/Fe] with NLTE
	8	4	NGC 5822	0.0	$\langle[S/Fe]\rangle \approx -0.02$	√	–
	8	7	NGC 2477	0.0	$\langle[S/Fe]\rangle \approx -0.04$	√	–
Kacharov et al. (2015)	3	6	M4	−1.08	$\langle[S/Fe]\rangle = +0.58 \pm 0.20$	√	no S-Na corr.
	3	6	M22	$-1.9 < [Fe/H] < -1.6$	$\langle[S/Fe]\rangle = +0.57 \pm 0.19$	√	1 star high [S/Fe], no S-Na corr.
	3	3	M30	−2.3	$\langle[S/Fe]\rangle = +0.55 \pm 0.16$	√	1 stars high [S/Fe], no S-Na corr.
Skúladóttir et al. (2015)	1	85	Sculptor dSph	$-2.5 < [Fe/H] < -2.0$	$[S/Fe] \approx +0.16$	√	NLTE included
				$-2.0 < [Fe/H] < -0.8$	[S/Fe] decreasing w/ increasing [Fe/H]	√	NLTE included

ISM of formation of these stellar populations (e.g. see Berg et al. 2015, for a recent comparison).

However, [Zn/Fe] is not constant at different [Fe/H] for stars in the thin and thick disks (Prochaska et al. 2000; Reddy et al. 2003, 2006; Bensby et al. 2003, 2005, 2013, 2014; Allende Prieto et al. 2004, the Galactic halo (Primas et al. 2000; Bihain et al. 2004; Cayrel et al. 2004; Nissen et al. 2004), 2007; Bonifacio et al. 2009), the bulge (Barbuy et al. 2015), and nearby dwarf galaxies (Sbordone et al. 2007; Venn et al. 2012; Skúladóttir et al., in prep.). This implies that zinc is not necessarily a good tracer of iron and that its nucleosynthetic origin is probably more complex than previously thought.

More specifically, the observed [Zn/Fe] is super-solar in the Milky Way halo, reaching $[Zn/Fe] \approx +0.5$ at $[Fe/H] < -3$ (Cayrel et al. 2004; Nissen et al. 2007). In the thin and thick disks, [Zn/Fe] decreases with increasing metallicity, reaching the solar ratio at $[Fe/H] \approx 0$ similar to the α-elements (Reddy et al. 2003, 2006; Bensby et al. 2003, 2005, 2013, 2014). Furthermore, Nissen & Schuster (2011) identified two populations in the solar neighbourhood with low- and high-α abundances, which also showed low and high ratios of [Zn/Fe], respectively. In the dwarf galaxies Sagittarius, Carina and Sculptor, measurements of [Zn/Fe] have revealed sub-solar ratios and possible scatter (Sbordone et al. 2007; Venn et al. 2012; Skúladóttir et al., in prep.). While there are only very sparse measurements of Zn in ultra-faint dSphs to date, the few data above $[Fe/H] > -2.2$ that overlap with our sampled range agree with our Galactic stars. Likewise, the remainder of the very metal-poor ultra-faint dSph stars with $[Fe/H] < -2$ fully agree with the metal-poor halo (Frebel et al. 2010, 2014, 2016; Roederer et al. 2016; Ji et al. 2016).

The fact that [Zn/Fe] increases at low metallicities, albeit at much lower metallicities than does the [α/Fe] ratio, seems to suggest a related origin of α-elements and Zn. However, predicted zinc yields of SNe Type II are too low to be compatible with ratios of $[Zn/Fe] \gtrsim 0$ (Nomoto et al. 1997a). By invoking models of core collapse SNe with high explosion energy, that is, hypernova, which are predicted to produce high levels of zinc, Kobayashi et al. (2006) were able to reproduce the trend observed in the disk. This does not, however, explain

the high levels of [Zn/Fe] at the lowest metallicities observed in the Milky Way halo. To produce the decreasing trend with metallicity, the ratio of [Zn/Fe] in SNe Type Ia yields should be even lower, and they are indeed predicted to be extremely low (Iwamoto et al. 1999). In addition to hypernova and SNe Type II, other production sites of zinc have been proposed, such as neutrino-driven winds (Hoffman et al. 1996) and the weak and/or main *s*-processes, but these are not expected to be dominant sources of zinc in the Milky Way (Mishenina et al. 2002; Travaglio et al. 2004).

Furthermore, there is still no clear consensus on the observed zinc abundances at the highest metallicities ([Fe/H] $\gtrsim$ 0). Some studies have reported an increase in [Zn/Fe] with [Fe/H] at this metallicity (Bensby et al. 2003, 2005; Allende Prieto et al. 2004), while others suggest a flatter trend (Pompéia 2003; Reddy et al. 2003, 2006; Bensby et al. 2013, 2014). Barbuy et al. (2015) observed red giant stars in the Milky Way bulge, and found a spread of $-0.6 <$ [Zn/Fe] $< +0.15$ for [Fe/H] ≥ -0.1, which has not been observed in dwarf stars. On the other hand, Takeda et al. (2016) did not find any significant scatter, nor a discrepancy of measured zinc abundances between field dwarf and giant stars in this same metallicity range.

The role of the *Gaia*-ESO Survey. The GES provides us with a large, homogeneous sample of Galactic stars that can help us to understand the Galactic chemical evolution of sulphur and zinc around solar metallicity. The only features of S I observable in the VLT-UVES (Dekker et al. 2000) ranges observed by GES (415−621 nm or 472−683 nm, red arm 520 nm and 580 nm standard settings, respectively) are weak, and belong to Mult. 8, which comprises three features, each consisting of a triplet. Due to the relatively low signal-to-noise ratio (S/N) and the relatively low resolving power ($R \approx 47\,000$) of the observed spectra, only the stronger sulphur triplet at 675.7 nm is useful for abundance determination in this case. As stated by Korotin (2009), NLTE effects are relatively small for this triplet, making our data very useful for this work. Two Zn I lines are observable in the wavelength range, at 481.0 and 636.2 nm.

The structure of the paper is as follows: in Sect. 2, we describe the data. Section 3 presents the chemical abundance analysis for each element and some specific findings, while in Sect. 4 we discuss these findings and summarise our results.

2. The *Gaia*-ESO data

The GES is one of ESO's large public spectroscopic surveys. It is an ambitious project that aims at collecting and analysing high-quality spectra for about 10^5 stars by the time the survey is completed, which will complement the spectroscopic capabilities of the *Gaia* satellite (Gaia Collaboration 2016) at faint magnitudes. The GES provides high-quality information about the kinematics and chemistry of the Milky Way bulge, the thin and thick disk, the halo and of a selected sample of about 60 open clusters covering a range of ages and masses. Additionally, data is collected for a number of clusters and benchmark stars for calibration purposes (Pancino et al. 2017). The project is run at the Paranal Observatory in the Chilean Andes, using the FLAMES (Pasquini et al. 2002) multi-object facility mounted at the UT2 telescope of the VLT.

The data analysed in the present paper belong to the fourth internal release (henceforth iDR4). iDR4 includes observations from the beginning of the survey (31 December 2011) until the end of July 2014. In this paper, only the UVES part of the collected data is considered. UVES observations are conducted mainly with the 580 nm setup which covers the wavelength range 472−683 nm. The fiber target allocation is summarised in Smiljanic et al. (2014), Stonkutė et al. (2016). F- and G-type dwarf stars are the primary targets in solar neighbourhood fields and should cover distances up to 2 kpc from the Sun, while a smaller selection of giants extends to larger distances. In globular clusters, all the targets belong to the red giant branch (RGB) or the red clump. In open clusters, red clump stars are the main UVES targets in old and intermediate age open clusters, with F-G dwarfs also being observed mainly in young clusters, and close intermediate-age ones. The data reduction of the UVES spectra (Sacco et al. 2014) makes use of the ESO FLAMES-UVES CPL pipeline[5]. A detailed description of the structure of the GES UVES sample, and of the strategy adopted to analyse it, is presented in Smiljanic et al. (2014).

Table 3. S I and Zn I lines analysed in this work.

Element	λ [nm]	$E_{\rm low}$ [eV]	log gf
S I	675.6750	7.87	−1.67
S I	675.6960	7.87	−0.83
S I	675.7150	7.87	−0.24
Zn I	481.0528	4.078	−0.16
Zn I	636.2338	5.796	+0.14

3. Chemical abundance analysis

The UVES spectra have been analysed using the multiple pipelines strategy described in Smiljanic et al. (2014). The individual results of the pipelines are combined with an updated methodology to define a final set of recommended values of the atmospheric parameters and abundances (see Casey et al. in prep.). We adopted here the homogenised stellar parameters from GES iDR4.

With fixed stellar parameters (effective temperature, surface gravity, micro-turbulence and [Fe/H]) at the values derived in the homogenised iDR4, we ran MyGIsFOS (Sbordone et al. 2014) to derive A(S) from a line profile fitting of S I Mult. 8, located at 675 nm. We chose to redetermine S abundances rather than employ the GES homogenised values due to an extra S I component mistakenly introduced in the second version of the GES linelist, which would skew the homogenised results towards lower S abundances.

A grid of synthetic spectra computed with turbospectrum (Alvarez & Plez 1998; Plez 2012), based on the grid of OSMARCS models provided by the GES collaboration (Smiljanic et al. 2014), were fit to the observed S I triplet. The employed atomic data are presented in Table 3. The log gf of the S I components used by Takeda et al. (2016) are slightly larger than the values chosen by the GES collaboration and correspond to a global log gf about 0.01 dex larger. The values suggested in NIST provide a global log gf 0.11 dex lower, which would provide larger sulphur abundances. A comparison of the GES homogenised S abundances with the one we derived (giving a systematic difference of −0.03 dex) is presented in Fig. 1. The S abundances we derived are made available at the CDS.

We visually inspected all the UVES spectra of F, G, and K stars, and retained spectra for which a safe measurement of

[5] http://www.eso.org/sci/software/pipelines/

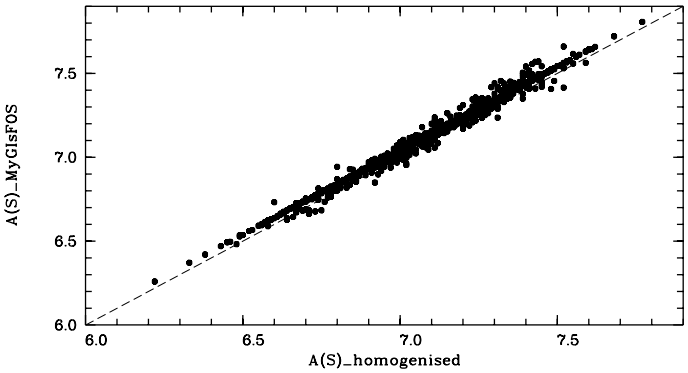

Fig. 1. Comparison of the A(S) values found in the present work versus the homogenised values provided by the GES. The systematic average difference among the two abundances is at −0.03 dex; small compared to the typical uncertainties in the abundance determination.

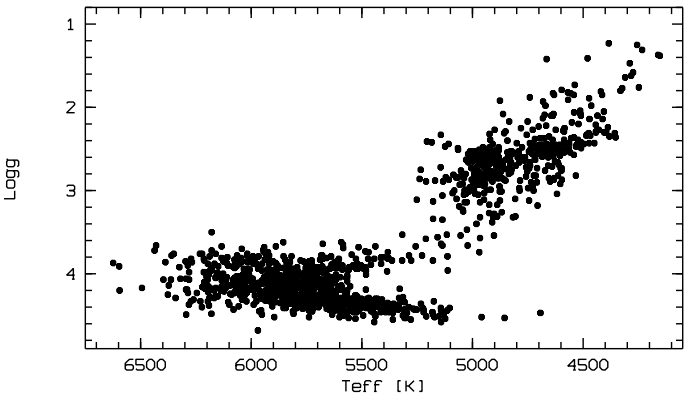

Fig. 2. Stars analysed in this work shown in the $T_{\rm eff}$ vs. log g plane.

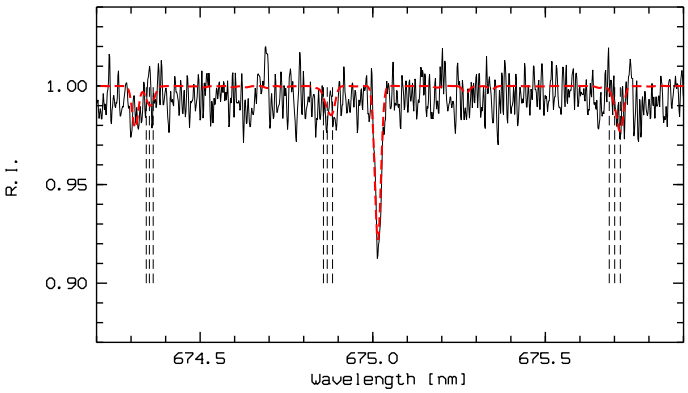

Fig. 3. Observed spectrum (solid black) of the star 21300738+1210330 in the range of the Mult. 8 of sulphur. A synthetic (dashed red) spectrum with a derived sulphur abundance of A(S) = 6.26 by the analysis is also included. Vertical dashed black lines highlight the positions of the S I lines of the Mult. 8.

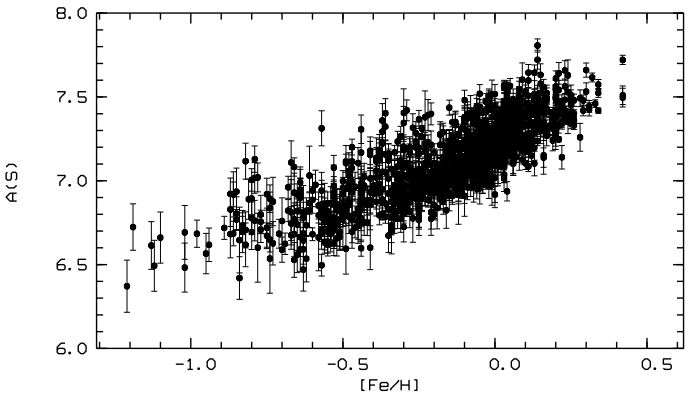

Fig. 4. A(S) vs. [Fe/H]. Error bars take into account 3σ uncertainty due to spectral S/N and derived using Cayrel's formula.

the S I line could be made. We ended up with a sample of 1301 stars. Our sample spans 2741 K in effective temperature (4153 ≤ $T_{\rm eff}$ ≤ 6624 K), 3.45 dex in surface gravity (1.23 ≤ log g ≤ 4.68), and 1.68 dex in metallicity (−1.07 < [Fe/H] < +0.61). In Fig. 2, the effective temperature and surface gravity of our sample of stars are shown. To assure us that this way of selecting stars did not introduce a bias, we compared [Zn/Fe] in the complete sample and the selected ones; we found no systematic difference (see Sect. 3.3).

One star (21300738+1210330, a member of the cluster M 15) with [Fe/H] = −2.65, shows a feature at the wavelength of the sulphur triplet (see Fig. 3) but due to a S/N of 100, which is low when compared to the weak line, we cannot exclude this as a spurious result.

We have relied on the homogenised abundances provided by iDR4 for zinc (and also compared to the abundances from our MyGIsFOS node) and the other elements shown here. The abundances are derived from two Zn I lines at 481.0 and 636.2 nm. For the majority of the stars in the sample, zinc abundances are derived from both lines, but for 92 stars the abundances rely on a single Zn I line. The zinc lines used are listed in Table 3. The 636.2 nm line is affected by the Ca I 636.1 nm auto-ionisation line and also blending CN lines (see Barbuy et al. 2015, for a discussion).

The solar abundances we have used for reference in our analysis are presented in Table 4. In the table we also provide the corresponding iDR4 recommended values from a GES analysis of an UVES solar spectrum.

Table 4. Solar abundances used in this work compared with GES homogenised values.

Element	GES iDR4	Adopted	Reference
A(Fe)	7.43	7.52	Caffau et al. (2011)
A(S)	7.03	7.16	Caffau et al. (2011)
A(Zn)	4.47	4.62	Lodders et al. (2009)
A(Ca)	6.21	6.33	Lodders et al. (2009)
A(Na)	6.21	6.30	Lodders et al. (2009)

3.1. Sulphur

The spectra we investigate are usually of good quality. For the spectra for which we derive sulphur abundance, we have a mean signal-to-noise ratio of $\langle S/N \rangle$ = 76 at 580 nm in the sample of spectra, with a dispersion around the mean value of 19. Only 37 spectra have a S/N lower than 40. The S/N induces an uncertainty on the sulphur abundance that we quantify with Cayrel's formula (Cayrel 1988), and by taking a 3σ interval we obtain an average uncertainty of 0.065 ± 0.032 dex. In Fig. 4 the abundance of sulphur is displayed as a function of the stellar metallicity and the error bars refer to the uncertainty related to the S/N.

The uncertainties in the stellar parameters lead to an uncertainty in the sulphur abundance determination. We considered five representative stars and derived the impact of changes in

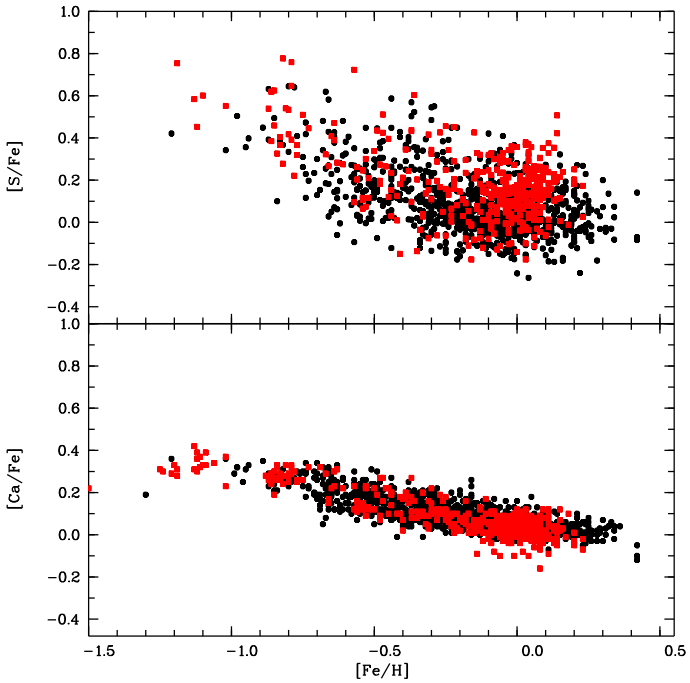

Fig. 5. [S/Fe] vs. [Fe/H] (*upper panel*) compared to [Ca/Fe] vs. [Fe/H] (*lower panel*). Black filled circles refer to dwarfs while red filled squares refer to giant stars. Error bars are not included for clarity, but they are presented in Fig. 6.

Table 5. Uncertainties on A(S) related to uncertainties in the stellar parameters.

Stellar parameters ($T_{\rm eff}$ /log g/[Fe/H])	ΔA(S) ±100 K	ΔA(S) ±200 K	ΔA(S) ±0.2 dex	ΔA(S) ±0.4 dex
4700/2.5/–0.25	−0.09 +0.10	−0.12 +0.23	+0.06 −0.06	+0.13 −0.11
4950/2.6/–0.30	−0.08 +0.10	−0.16 +0.23	+0.06 −0.07	+0.14 −0.15
5300/4.4/–0.50	−0.09 +0.07	−0.13 +0.16	+0.10 −0.11	+0.24 −0.19
5800/4.3/+0.0	−0.06 +0.06	−0.11 +0.13	+0.07 −0.07	+0.15 −0.13
6300/4.1/–0.30	−0.04 +0.04	−0.07 +0.09	+0.06 −0.06	+0.10 −0.10

$T_{\rm eff}$ and log g on the determination of A(S). The results are presented in Table 5. The uncertainties associated with temperature and gravity in the iDR 4 sample are 112 K and 0.22 dex, respectively. Propagation of these errors implies an uncertainty in A(S) of about ±0.10 dex in both cases.

Figure 5 depicts the [Ca/Fe] versus [Fe/H] (provided by the iDR 4 of the GES), which is a typical and well studied α-element, and of sulphur. Figure 6 is the same as the top panel of Fig. 5 but includes the proper NLTE corrections we computed with the model atom described in Korotin (2008, 2009), which are small and negative; the maximum absolute value is −0.071 and on average $\langle {\rm NLTE_{cor}} \rangle = -0.023 \pm 0.011$. As expected, [S/Fe] is close to zero for solar-metallicity stars, and it increases as the metallicity is reduced.

The absolute value of NLTE corrections increases as the temperature increases achieving the maximum value at $T_{\rm eff}$ = 6000−6500 K. Corrections increase as well when decreasing gravity and can exceed 0.1 dex. Since our program giants have relatively low temperatures, the NLTE corrections are small in this case.

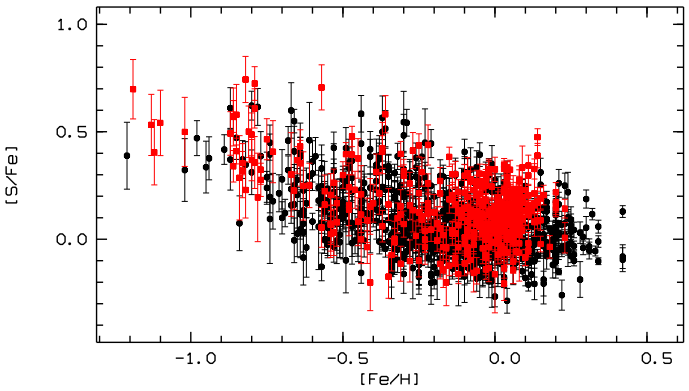

Fig. 6. [S/Fe] vs. [Fe/H] for the sample stars including NLTE corrections. Black and red symbols represent dwarf and giant stars, respectively, and we see no difference in the two populations.

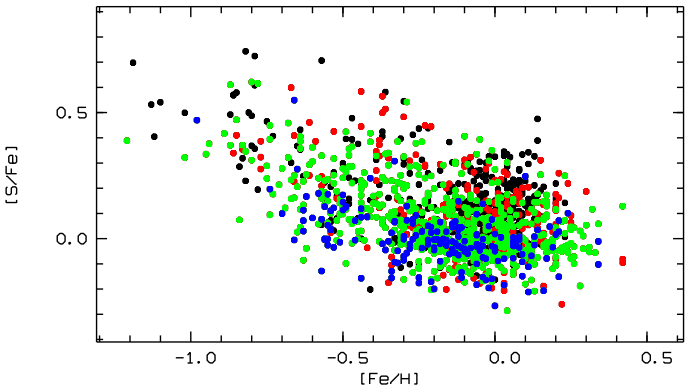

Fig. 7. [S/Fe] vs. [Fe/H] for the complete sample of stars: black, stars cooler than 5000 K; red 5000 ≤ $T_{\rm eff}$ < 5500 K; green 5500 ≤ $T_{\rm eff}$ < 6000 K; blue hotter than 6000 K.

Caffau et al. (2007) investigated granulation effects for the S I 675.6 nm triplet in a few solar-metallicity stars and found that the effects are small.

We have noticed that cool stars around solar metallicity tend to give a higher [S/Fe] than hotter ones. This is summarised in Fig. 7 where stars in different ranges in $T_{\rm eff}$ are shown with different colours. On average, the lower the temperature, the higher the [S/Fe]. We think this may be related to the CN lines that are perhaps not properly taken into account in the wavelength range of the S I feature in the GES line-list. This effect can have an impact on the analysis of the open clusters in which mainly cool dwarfs and giants have been observed.

At odds with the results presented by Nidever et al. (2014), Hayden et al. (2015) from APOGEE data, our data show no indication of two different sequences in the [α/Fe] vs. [Fe/H] planes for sulphur or calcium (see Fig. 5). The APOGEE samples and ours may cover overlapping regions in terms of galactocentric distances and heights over the galactic plane (see Figs. 14 and 15). A detailed comparison is, however, not possible. In fact, the trends detected in the APOGEE samples make use of a [α/Fe] parameter obtained by combining measures of O, Mg, Si, Ca, Ti and S. Calcium and sulphur abundances presented by Holtzman et al. (2015, see their Fig. 14) show trends qualitatively similar to ours. Additionally, the APOGEE sample sizes are significantly larger than ours.

In the sample of stars we analysed there are 54 stars that have been observed as being members of globular clusters, and

Table 6. Distances, [Fe/H], [S/Fe], and [Zn/Fe], for stars belonging to clusters.

Cluster	Type	$R_\odot$	R_{GC}	[Fe/H]	[S/Fe]	[S/Fe]$_{NLTE}$	[Zn/Fe]	[Zn/Fe]$_{NLTE}$	Stars		Comment
		kpc	kpc						N	Type	
NGC 104/47 Tuc	GC	4.5	7.3	−0.81 ± 0.04	+0.51 ± 0.14	+0.46 ± 0.14	+0.18 ± 0.11	+0.17 ± 0.10	19	G	
NGC 1851	GC	12.1	16.6	−1.13 ± 0.01	+0.52 ± 0.09	+0.47 ± 0.09	+0.23 ± 0.01	+0.20 ± 0.01	2	G	
NGC 2808	GC	9.6	11.1	−1.15 ± 0.06	+0.68 ± 0.11	+0.62 ± 0.11	+0.06 ± 0.01	+0.05 ± 0.01	2	G	high S
M 15	GC	10.4	10.4	−2.65	+1.75	+1.68	+0.16	+0.17	1		
NGC 362	GC	8.7	9.40	−1.02	+0.55	+0.50	−0.01	−0.01	1	G	high S
M 67	OC	0.775	8.49	−0.12 ± 0.04	+0.02 ± 0.06	−0.01 ± 0.06	−0.03 ± 0.08	−0.06 ± 0.08	18	D,G	G with high S
NGC 2243	OC	3.45	10.1	−0.55 ± 0.04	+0.15 ± 0.07	+0.11 ± 0.07	+0.04 ± 0.05	−0.00 ± 0.05	9	G	
Berkeley 25	OC	9.1	15.6	−0.45	+0.12	+0.08	+0.12	+0.06	1	G	
NGC 2451A	OC	0.2	8.0	−0.05 ± 0.06	+0.03 ± 0.11	+0.01 ± 0.12	−0.02 ± 0.08	−0.04 ± 0.08	2	D	
NGC 2516	OC	0.35	7.93	−0.09 ± 0.04	+0.21 ± 0.08	+0.20 ± 0.08	+0.48 ± 0.10	+0.46 ± 0.10	2	D	high S
NGC 2547	OC	0.36	7.98	−0.12 ± 0.03	+0.05 ± 0.09	+0.02 ± 0.09	+0.04 ± 0.04	+0.02 ± 0.04	2	D	
IC 2391	OC	0.15	7.94	−0.16	+0.13	+0.11	+0.12	+0.10	1	D	
Trumpler 20	OC	3.0	6.9	+0.01 ± 0.05	+0.10 ± 0.09	+0.07 ± 0.09	−0.27 ± 0.12	−0.34 ± 0.12	39	G	
NGC 4815	OC	2.5	6.9	−0.11 ± 0.02	+0.16 ± 0.05	+0.12 ± 0.05	−0.23 ± 0.16	−0.31 ± 0.16	5	G	high S
Pismis 18	OC	2.2	6.8	−0.01 ± 0.03	+0.12 ± 0.06	+0.09 ± 0.06	−0.28 ± 0.11	−0.35 ± 0.11	6	G	
NGC 6005	OC	2.7	5.9	+0.06 ± 0.02	+0.14 ± 0.09	+0.12 ± 0.09	−0.31 ± 0.09	−0.37 ± 0.09	12	G	
Trumpler 23	OC	2.0	6.3	+0.05 ± 0.04	+0.27 ± 0.07	+0.24 ± 0.07	−0.21 ± 0.19	−0.27 ± 0.18	10	G	high S
NGC 6633	OC	0.38	7.64	−0.15 ± 0.06	+0.04 ± 0.04	+0.01 ± 0.03	−0.09 ± 0.05	−0.12 ± 0.08	8	D,G	
NGC 6705	OC	1.9	6.3	+0.02 ± 0.06	+0.20 ± 0.10	+0.16 ± 0.10	−0.28 ± 0.18	−0.37 ± 0.17	19	G	trend S with T_{eff}
Berkeley 81	OC	3.0	5.7	+0.10 ± 0.06	+0.19 ± 0.11	+0.16 ± 0.11	−0.36 ± 0.16	−0.42 ± 0.15	6	G	trend S with T_{eff}
NGC 6802	OC	1.8	7.1	−0.00 ± 0.02	+0.09 ± 0.07	+0.05 ± 0.07	−0.15 ± 0.13	−0.22 ± 0.13	9	G	

Notes. Globular cluster distances from Harris (1996; 2010 edition). For open clusters: distance for NGC 2243, Bragaglia & Tosi (2006); Be 25, Carraro et al. (2007); M 67, Montgomery et al. (1993); all the others from Spina et al. (2017, and reference therein). Galactocentric radii have been computed assuming a distance of the Sun to the Galactic centre of 7.94 kpc (Eisenhauer et al. 2003). [Fe/H] is derived averaging among the selected stars in each cluster. The solar abundances applied here are those of the third column in Table 4. Average [Fe/H] values for the open clusters are about 0.1 dex below those reported by Jacobson et al. (2016) and Spina et al. (2017) due to the use of different solar reference values and to the inclusion of only the subset of stars with measured sulphur.

312 members of open clusters. We verified the membership comparing radial velocities and metallicities. For the young clusters we considered the members identified by Spina et al. (2017), which were selected based on surface gravity and lithium line strength. We could derive the sulphur abundance in 21 clusters, 20 of which were analysed for the first time, as well as 47 Tucanae, for which we already had a sulphur determination (Sbordone et al. 2009). A more detailed discussion on this cluster is presented in Sect. 3.2. Table 6 provides S and Zn abundances for each cluster.

For some open clusters (e.g. Trumpler 20, Trumpler 23, NGC 6705, Berkeley 81) the high [S/Fe] could be explained by the low T_{eff} of the member stars. This is in line with what was found in M 67 for which, when selecting only the stars with $T_{eff} > 5000$ K, we have a smaller star-to-star scatter, [S/Fe] = +0.0 ± 0.02. Also the 19 giant members of NGC 6705 show a clear trend of increasing [S/Fe] by decreasing the stellar effective temperature. The effect is evident in Fig. 8. However, this cannot explain the high [S/Fe] = +0.21 of NGC 2516 from two relatively warm stars ($T_{eff} > 5500$ K).

In Fig. 9 we compare the [S/Fe] versus [Fe/H] relation from the literature for open and globular clusters to our measurements after NLTE corrections are applied to our sulphur values. This figure is an update from our work in Caffau et al. (2014).

3.2. A possible S – Na correlation in 47 Tucanae

Sulphur abundances in NGC 104 (47 Tuc) were investigated by Sbordone et al. (2009). They determined sulphur abundances in four turn-off- and five subgiant stars using VLT-UVES spectra and measuring lines of S I Mult. 1 around 922 nm. They claimed a statistically significant positive correlation of [S/Fe] with [Na/Fe], which, if confirmed, would be of high interest in the context of the investigation of multiple populations in globular clusters, especially because there is no obvious mechanism of sulphur production as part of any currently considered globular cluster self-enrichment mechanisms (Sbordone et al. 2009).

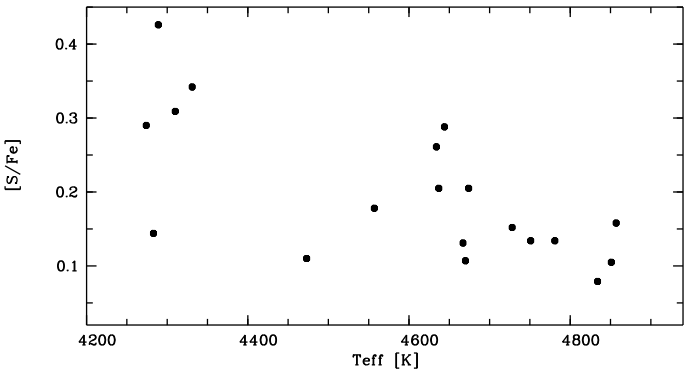

Fig. 8. [S/Fe] versus effective temperature for the 19 stars in NGC 6705.

In Fig. 10 we plot [S/Fe] vs. [Na/Fe] in NGC 104 for the Sbordone et al. (2009) sample together with the current one. The Sbordone et al. (2009) abundance ratios have been brought into the same scale used in GES by accounting for the slightly different assumed solar abundances.

When looking at the Sbordone et al. (2009) and GES samples separately, neither produces a significant slope when fitted

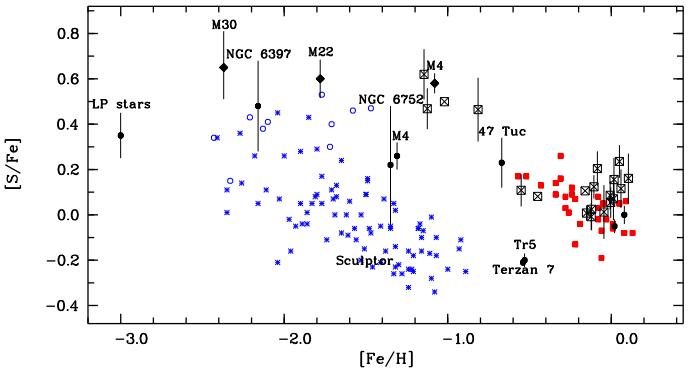

Fig. 9. [S/Fe] vs. [Fe/H] for the star members of open and globular clusters, compared to analysis of clusters and field stars available in the literature. This is an update of Fig. 4 of Caffau et al. (2014), see references therein. For added samples: crossed black squares are from this work, blue stars are stars belonging to Sculptor dSph from Skúladóttir et al. (2015), open blue circles are field stars from Jönsson et al. (2011), and red filled squares are field stars from Ecuvillon et al. (2004).

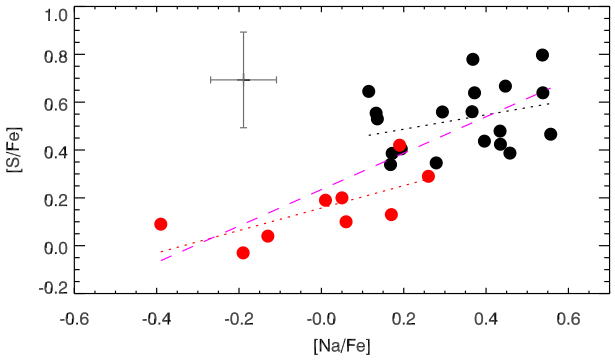

Fig. 10. [S/Fe] vs. [Na/Fe] for stars in NGC 104. Black points are GES measurements in giants, and red points are Sbordone et al. (2009) TO and SGB stars shifted to our adopted solar abundance scale. Linear fits are included, the magenta line indicating the fit to the whole sample. A conservative error estimate is also shown.

linearly (GES, 0.30±0.34, Sbordone et al. 2009 0.47±0.37). The Sbordone et al. (2009) sample showed a very high likelihood of correlation between [S/Fe] and [Na/Fe] through a Kendall τ test. However, when the two samples are taken together, the slope of the linear fit is highly significant (0.76 ± 0.18). Also, it is remarkable how the two samples cover different ranges in [Na/Fe]. The GES sample appears to cover a range consistent with recent [Na/Fe] measurements in NGC 104 giants (Cordero et al. 2014; Thygesen et al. 2014; Johnson et al. 2015), while analyses of TO and SGB stars find a distribution significantly more extended towards low Na abundances (Dobrovolskas et al. 2014; Marino et al. 2016). It is particularly intriguing that when stars belonging to the bright and faint SGB of 47 Tuc (bSGB, fSGB) are discriminated in Marino et al. (2016), the bSGB stars appear Na-poor, and match the range in Na observed by Dobrovolskas et al. (2014) and Sbordone et al. (2009). The fSGB stars, on the other hand, match the Na abundances covered in the GES sample and other RGB-based studies. On the one hand, the bSGB is more populated and brighter so it is reasonable that the Sbordone et al. (2009) and Dobrovolskas et al. (2014) samples, designed to study the weak Li I 670.8 nm doublet, were drawn from this population. On the other hand, it is unclear why RGB samples appear to lack the Na-poor tail detected in the prominent bSGB. Investigating the [Na/Fe] distributions of different NGC 104 populations is outside the scope

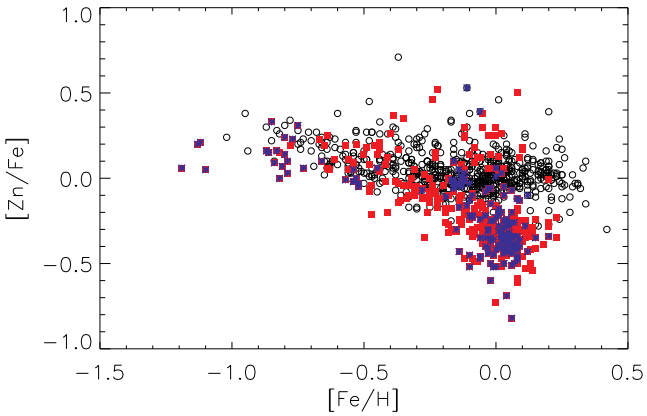

Fig. 11. [Zn/Fe] vs. [Fe/H] for the sample stars analysed for sulphur. Dwarf stars are represented as black open circles, giant stars as red squares, and stars in clusters as blue crosses.

of the present paper, but the similarity between the [Na/Fe] distribution in the two NGC 104 SGBs, and the two samples investigated here for sulphur and zinc, suggest the possibility that the Sbordone et al. (2009) and the GES samples might be drawn from different subpopulations of the cluster, each without internal [S/Fe] spread, but rather characterised by different [S/Fe] values. In this case, once the Sbordone et al. (2009) sample is brought to the solar abundance scale employed in our analysis, they would correspond to [S/Fe] = 0.16 ± 0.14 and [S/Fe] = 0.53 ± 0.13 (Sbordone et al. 2009, GES).

Caution in the comparison is in order since different multiplets are used, as well as stars of different atmospheric parameters, so systematic differences between the two samples might be induced if line formation systematics (3D, NLTE...) are not correctly accounted for. However, the currently available data indicate that NGC 104 displays either a spread in [S/Fe], strongly correlating with [Na/Fe], or two subpopulations characterised by significantly different values of [S/Fe].

3.3. Zinc over iron

In Fig. 11 we show the [Zn/Fe] versus [Fe/H] for the sample of stars analysed for sulphur. A large scatter in [Zn/Fe] is evident overall around solar metallicity. When we divide the sample into dwarf stars ($\log g > 3.45$) and giant stars we realise that the large spread is mainly due to giants. The 897 stars classified as dwarfs give $\langle[\mathrm{Zn/Fe}]_\mathrm{d}\rangle = 0.07 \pm 0.11$ while the 404 giants give $\langle[\mathrm{Zn/Fe}]_\mathrm{g}\rangle = -0.12 \pm 0.22$. Hence, the scatter of [Zn/Fe] for giant stars is larger than both the observational error, which is on average ≈0.12 (Fig. 11), and the dispersion observed within dwarf stars. On average, giants show lower [Zn/Fe] than dwarfs. Such differences are even more evident when we select the 525 stars around solar metallicity, $-0.1 < [\mathrm{Fe/H}] < +0.1$, for which we derive $\langle[\mathrm{Zn/Fe}]\rangle = -0.06 \pm 0.19$. In this case the 295 dwarfs contribute with $\langle[\mathrm{Zn/Fe}]_\mathrm{d}\rangle = 0.04 \pm 0.10$ and the 230 giants with $\langle[\mathrm{Zn/Fe}]_\mathrm{g}\rangle = -0.20 \pm 0.20$. The same calculations for the 162 stars (mainly giants) that are members of clusters provide $\langle[\mathrm{Zn/Fe}]_\mathrm{c}\rangle = -0.19 \pm 0.22$ for the overall sample, and $\langle[\mathrm{Zn/Fe}]\rangle = -0.20 \pm 0.20$ for stars around solar metallicity. Stars in clusters contribute to lowering the average [Zn/Fe] of the giant sample at [Fe/H] ≈ 0.0 but apparently they are not the main drivers of the large scatter, as can be seen in Fig. 11.

To investigate if the differences between dwarfs and giants are real or if the observed trend is driven by analysis and/or observational biases, we made several tests.

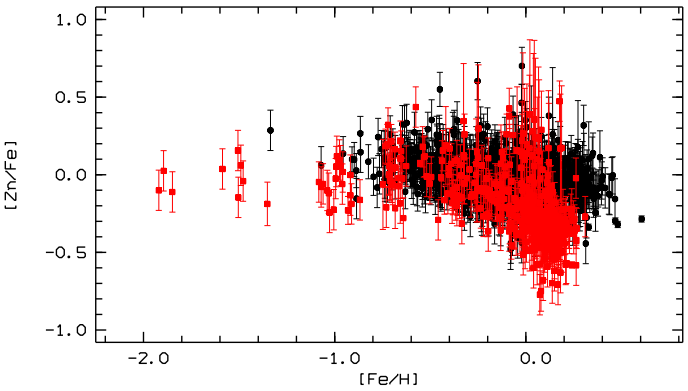

Fig. 12. [Zn/Fe] vs. [Fe/H] for the complete GES sample stars with detection of zinc. Black filled circles represent dwarf stars and red filled squares represent giant stars.

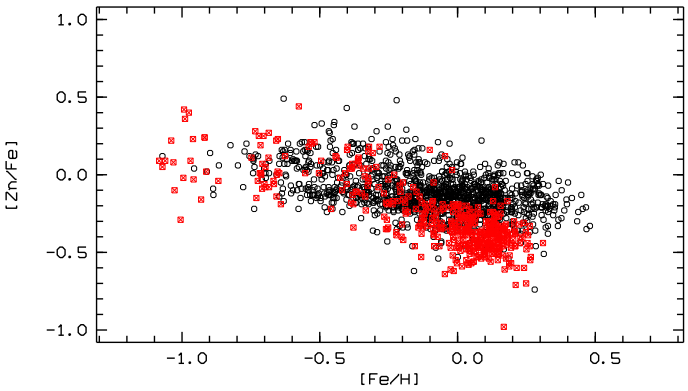

Fig. 13. [Zn/Fe] vs. [Fe/H] in the case of zinc derived with MyGIsFOS only for the 481.0 nm line. Symbols are as in Fig. 11.

First, we checked if this behaviour is a consequence of restricting the GES sample to stars with detected sulphur. This is shown in Fig. 12, where we plot [Zn/Fe] versus [Fe/H] for the complete sample of 1724 stars. In the solar-metallicity regime we can see that both the low [Zn/Fe] values and the large scatter are clearly reproduced in the case of giant stars.

Second, we tested possible biases due to NLTE effects. Using the computations of Takeda et al. (2005) we could derive for our sample a NLTE correction of -0.06 ± 0.02 for zinc, which is well within the observational uncertainty. Furthermore the correction goes in the opposite direction, that is, it is negative, meaning that it further decreases the [Zn/Fe] value. For iron, we provide an estimate of the NLTE effects using the results of Mashonkina et al. (2011, see also Lind et al. 2012). According to their calculations, the NLTE correction, which mainly affects the Fe I lines, is smaller than 0.1 dex for both giants and dwarfs at solar metallicity, and is always positive. Thus, also in this case the NLTE effect is expected to be negligible and to depress the [Zn/Fe] values further on.

Third, to investigate the effects that granulations can have on the abundances we computed zinc abundances for 22 hydrodynamical models and their reference $1D_{LHD}$ models from the CIFIST grid (Ludwig et al. 2009), for two metallicities (0.0 and −1.0) and we computed the 3D correction as in Caffau & Ludwig (2007). To study the effects in dwarf stars, we selected the solar model and three effective temperatures (5500, 5900 and 6250 K) for two gravities (4.0 and 4.5). In all cases but one (for the 481 nm line and the hottest model at $\log g = 4.0$ and [Fe/H] = 0.0), the 3D corrections are positive, on average 0.08 and 0.06 for the 481 nm and 636 nm lines, respectively. For the giant stars we investigated three models at 5000 K (gravity of 2.5, 3.0 and 3.5) and two at 4500 K (gravity 2.0 and 2.5). The 3D corrections are slightly smaller for giants, 0.04 and 0.02 for the 481 nm and 636 nm lines, respectively. Hence, the granulation effects are also comparable to the uncertainties.

Fourth, we considered the zinc abundances derived by MyGIsFOS when fitting the strongest of the two Zn I lines at 481.0 nm. In principle, if there was a problem in the abundances derived from the 636.2 nm line, either due to the blending CN lines or to the Ca I 636.1 nm auto-ionisation line, we may expect a systematic difference. The result is shown in Fig. 13. We notice that, although the star-to-star scatter is smaller than the homogenised A(Zn) values (by about 0.08 dex at metal-rich regime), the different behaviour of dwarfs and giants is still there, and in particular around solar-metallicity, giant stars show much lower [Zn/Fe] values than dwarfs. Furthermore, opposite to the case of sulphur (Fig. 8), a clear trend of increasing/decreasing zinc abundance as a function of the effective temperature is not evident. We also selected giant stars similar in stellar parameters but with a difference of at least 0.4 dex in [Zn/Fe] and compared the observed spectra and checked the results we obtained from MyGIsFOS. The spectra of low- and high-Zn abundance stars appear similar and MyGIsFOS provides very similar values, close to the low measurement. This test leads us to have confidence in the presence of a population of giant stars with low-Zn abundance, while casting doubt on the high values provided in iDR4. This conclusion is reinforced by the absence of high-Zn-abundance giants in Fig. 13 when compared to Fig. 12. We suspect that the high [Zn/Fe] values are the result of an incorrect synthesis of the region around the Zn I 636.2 nm line in iDR4.

Finally, to investigate the impact of the uncertainties in the stellar parameters on [Zn/Fe], we took into consideration a giant star with a low-Zn abundance. With MyGIsFOS we derived the Fe and Zn abundances by changing effective temperature, gravity, and micro-turbulence according to their uncertainties. A change in ±110 K in $T_{\rm eff}$ implies a change in [Zn/Fe] by $^{-0.07}_{+0.08}$; by changing $\log g$ by ±0.22 the change in [Zn/Fe] is of ±0.03; a change in the micro-turbulence of $\pm 0.10 \mathrm{km\,s^{-1}}$ implies a change in [Zn/Fe] of about ∓0.02. All the changes in [Zn/Fe] are too small to alter the picture described above.

In conclusion, after all these tests, we believe it is unlikely that the difference in [Zn/Fe] between dwarfs and giants is due to some systematic error in the analysis. We therefore address the question of whether or not the two samples come from the same parent population.

3.4. Different populations and a possible radial gradient in [Zn/Fe]

The selection function specific to the GES UVES targets (Smiljanic et al. 2014) results in a magnitude-limited sample primarily aimed at local FGK dwarfs, while the (less numerous) giants generally reside at much larger distances from the Sun. The giant stars are also targeted on purpose with UVES in the bulge fields and in the CoRoT fields. In fact, of the giant sample, 20% are in the bulge direction (actually inner disk giants) and 10% in the CoRoT fields. This, combined with the open clusters, fully explains why the sample is strongly concentrated on the galactic plane. For the clusters, we took the distances from the literature (see Table 6). For the field stars, distance moduli were computed using a Bayesian method on the Padova

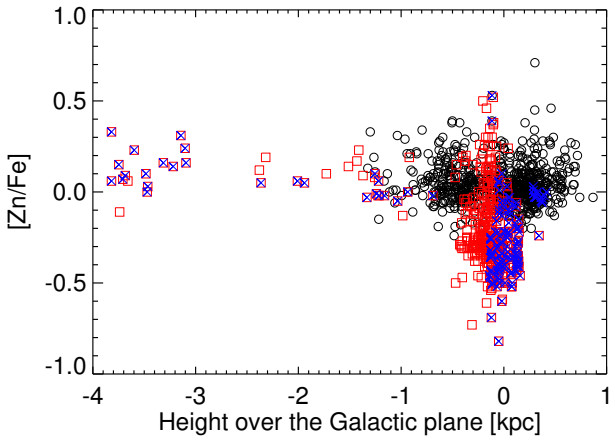

Fig. 14. [Zn/Fe] as a function of the height above (or below) the Galactic plane. Symbols are as in Fig. 11.

isochrones (Bressan et al. 2012, CMD 2.7) and using the magnitude independent of extinction $K_{J-K} = K - \frac{A_K}{A_J - A_K}(J-K)$ with extinction coefficients computed applying the Fitzpatrick & Massa (2007) extinction curve on the Castelli & Kurucz (2003) SEDs. The prior on the mass distribution used the IMF of Chabrier (2001) while the prior on age was chosen to be flat. Stars too far from the isochrones were rejected using the $\chi^2_{0.99}$ criterion. Moreover, giants were targeted predominantly in open clusters, or in globular clusters that were observed as calibrators (Pancino et al. 2017). The dwarf sample happens to be entirely located within ≤1.5 kpc from the Sun, with a peak of the distribution at $D \approx 0.5$ kpc. Giant stars cover a much larger range in distance, $0.0 < D/\mathrm{kpc} < 16$, with all stars but one (further than 6 kpc from the Sun), residing in clusters. Stars in the distant giants sample are all at low metallicity ([Fe/H] ≤ −0.5), and are almost entirely hosted in globular clusters. Local giants are predominantly metal-rich, and largely hosted in open clusters.

In Fig. 14 we show the [Zn/Fe] ratio as a function of the height of the stars from the Galactic plane. It is then obvious that the giant sample is more strongly concentrated on the Galactic plane, while dwarfs are mostly observed at heights larger than 0.5 kpc from the plane. If we select all dwarfs and giants with heights ≤1 kpc from the plane then the distribution of [Fe/H] of the two samples is distinctly different. Both dwarfs and giants have a peak at solar metallicity, yet the dwarfs have a large excess of lower metallicity stars down to [Fe/H] = −1.0. This suggests that our dwarf star sample is largely dominated by the thick disc objects, while the field giants and the open clusters are an almost pure thin disc population.

On average, giants have been observed with UVES in the GES at Galactic latitudes lower than dwarfs: $\langle|b|\rangle_G \approx 9°$, while dwarfs $\langle|b|\rangle_D \approx 30°$. This bias is not compensated by the geometrical bias: for a given apparent magnitude, giants are more distant, so that they are observed at larger heights from the Galactic plane than dwarfs of the same apparent magnitude and Galactic latitude. Of course the distinction between thin and thick discs, based only on the height from the Galactic plane, is very crude. The second *Gaia* data release will provide parallaxes and proper motions for all these stars. When coupled with our radial velocities, we shall be able to compute Galactic orbits for all these stars and classify them as belonging to the thin or the thick disc.

Following the findings of Fuhrmann (1998, 1999, 2004), that have been verified by subsequent investigations (see, e.g. Wojno et al. 2016; Haywood et al. 2016; Mikolaitis et al. 2014; Recio-Blanco et al. 2014, and references therein), one expects (kinematically selected) thin disc stars to have lower α-to-iron ratios than thick disc stars of the same metallicities. If our dwarf star sample were dominated by the thick disc stars, as suggested by Fig. 14, we would expect higher α-to-iron ratios than in the giant star sample. However, as can be appreciated in Fig. 5, there is no clear distinction between dwarfs and giants in the α-to-iron ratios.

In Fig. 15 we plot chemical abundances of giants, dwarfs, and stars in clusters as a function of their distance (from Table 6) from the Galactic centre. In panels a, c, and d of Fig. 15, we can see the dwarf sample (black open circles) located at around 8 kpc from the Galactic centre (where the Sun is situated), consistent in [Fe/H] and [Zn/H] with disc stars. Giant stars belonging to clusters (globular or open) are depicted in panels a, c, and d of Fig. 15 as red squares with blue crosses. In panel b we binned the abundances in various distance bins. For Galactocentric distances larger than 7.5 kpc, on average $\langle$[Zn/Fe]$\rangle \approx 0.0$, with a good agreement between field giants, giant stars in clusters, and dwarf stars. As we move to smaller distances from the Galactic centre, the giants and the cluster stars display a smaller $\langle$[Zn/Fe]$\rangle \approx -0.2$, while the dwarf stars remain at $\langle$[Zn/Fe]$\rangle \approx$ 0.0.

However, panels a and b in Fig. 15 do not allow us to disentangle the superimposed effects of metallicity and galactocentric distance. For this purpose, in Fig. 16 we plot [Zn/Fe] versus the galactocentric radius, but split the whole sample into four metallicity ranges. Once this is done, a few general behaviours of the sample appear with more clarity:

- At low metallicity ([Fe/H] < −0.5) both dwarfs and giants show slightly super-solar [Zn/Fe], constant at all galactocentric radii.
- As metallicity increases (−0.5 ≤ [Fe/H] < −0.25, and −0.25 ≤ [Fe/H] < 0), sub-solar [Zn/Fe] giants appear in the inner disk. The average value for dwarfs decreases to [Zn/Fe] ≈ 0. At the same time, at the solar radius there is little evidence of a discrepancy between dwarfs and giants.
- The most Zn-poor giants all appear at small galactocentric radii ($R_{GC} < 7$ kpc and for high metallicities ([Fe/H] > 0).

It thus appears that the dwarf-giants discrepancy in Figs. 11 to 15 is driven by the superposition of different selection effects. On the one hand, giant stars appear to be much more concentrated on the plane, thus likely belonging preferentially to a younger population than the dwarfs. On the other hand, Zn-poor giants appear to prevalently belong to the inner disk, and all display solar, or supersolar metallicities. Although it cannot be excluded that a systematic difference in the analysis exists between dwarfs and giants above [Fe/H] ≈ 0, due to the limited overlap in R_{GC} at high metallicity, the trend appears already quite evident in the −0.25 ≤ [Fe/H] < 0 bin, where there is a healthy sample of giants at higher galactocentric radii whose [Zn/Fe] is similar to that of the dwarfs. It is also worth noticing that there is a small subpopulation of dwarfs with low [Zn/Fe] but their small number (seven dwarfs with [Zn/Fe] < −0.3) prevents us from drawing any strong conclusion. These are prevalently cool dwarfs, hence faint ones, and closer to the galactic plane than the bulk of the dwarfs in our sample. We are thus inclined to consider the low [Zn/Fe] ratios we observe as a real signature of the chemical enrichment of the inner MW disk.

The complex behaviour of [Zn/Fe] with R_{GC}, metallicity, and age is shown in two recent investigations of high-precision abundances in nearby solar twins. Nissen (2015) analyses a sample of 21 solar twins and finds a clear trend in [Zn/Fe], which increases with increasing stellar age (by about 0.1 dex over about 8 Gyr).

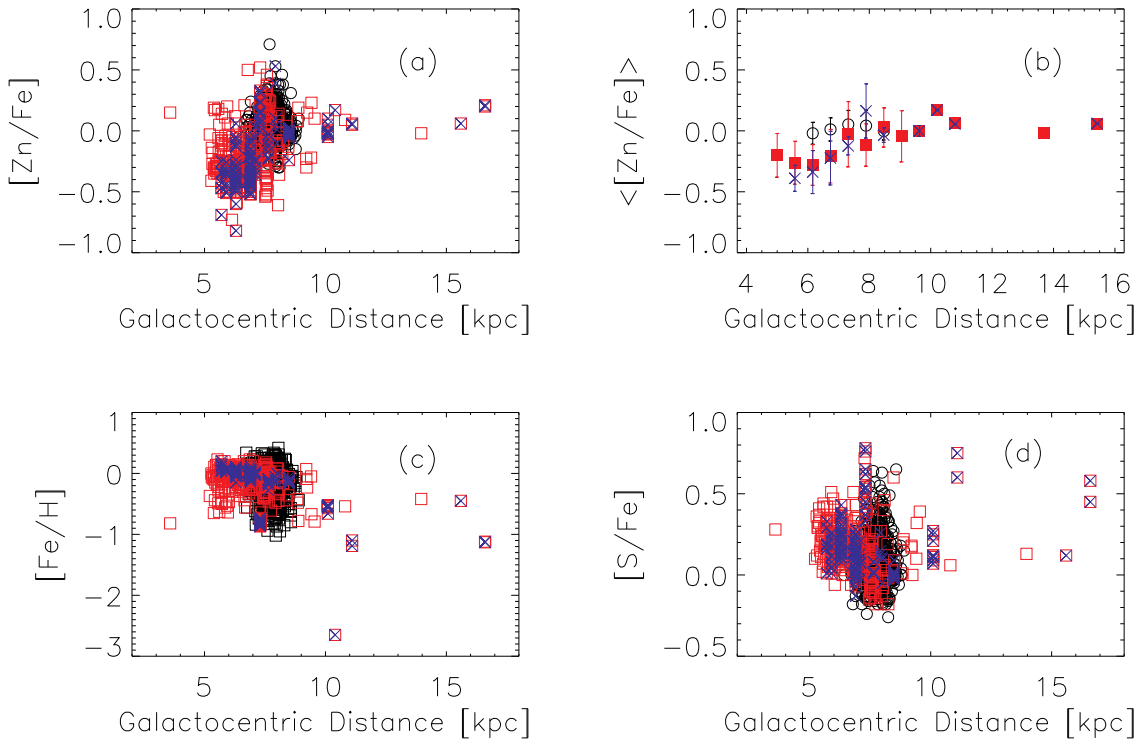

Fig. 15. *Panels a*, *c*, *d*: [Zn/Fe] *(a)*, [Fe/H] *(c)*, and [S/Fe] abundances *(d)* for the sample of stars analysed for sulphur as a function of their Galactocentric distance. Symbols are the same as in Fig. 11. *Panel b*: average [Zn/Fe] in different distance bins for dwarfs (black circles), giants (red squares) and for stars in clusters (blue crosses).

A similar trend is also found for [Mg/Fe] and [Al/Fe]. Similar results are found by Spina et al. (2016) in a study of nine objects. The much more heterogeneous, and lower quality GES sample cannot detect such subtle variations, and lacks precise age estimates. In Fig. 16, the distribution of solar-metallicity, solar-galactocentric-radius dwarfs disperse in [Zn/Fe] by a value comparable to the extent of the correlation found by Nissen (2015) (and Mg and Al have comparable dispersion). These works, however, support the finding of a dependency of [Zn/Fe] from the star formation epoch and environment that is on such stark display in our inner-disk giants.

3.5. A possible effect of SN Ia dilution

The concentration of low-[Zn/Fe] stars on the galactic plane and at small galactocentric radii suggests they might represent a younger population than the dwarf sample, whose Zn would then be more diluted by SN Ia ejecta (which are believed to be almost Zn-free). However, this said dilution would also affect α elements to some extent. We thus proceeded to test this scenario through a simple calculation. Inspecting Figs. 5 and 11, one notices that at $A(\mathrm{Fe}) = 7.22$ (i.e. [Fe/H] ≈ -0.3), giant and dwarf stars show on average the same ratios of alpha elements, in particular A(Ca)-A(Fe) and A(S)-A(Fe), along with (at or outside the solar circle) the same A(Zn)-A(Fe). Considering that:

$$A(\mathrm{Fe}) = \log \frac{N_{\mathrm{Fe}}}{N_{\mathrm{H}}} + 12 = \log \frac{N_{\mathrm{Fe}} \times m_{\mathrm{Fe}}}{N_{\mathrm{H}} \times m_{\mathrm{H}}} + 12 - \log \frac{m_{\mathrm{Fe}}}{m_{\mathrm{H}}} \quad (1)$$

$$\approx \log \frac{N_{\mathrm{Fe}} \times m_{\mathrm{Fe}}}{M_{\mathrm{g}}} + 12 - \log \frac{m_{\mathrm{Fe}}}{m_{\mathrm{H}}} = \log \frac{M_{\mathrm{Fe}}}{M_{\mathrm{g}}} + 12 - \log \frac{m_{\mathrm{Fe}}}{m_{\mathrm{H}}}, \quad (2)$$

where m_{Fe} (m_{H}) is the atomic mass of iron (hydrogen), and that

$$A(\mathrm{X}) - A(\mathrm{Fe}) = \log \frac{M_{\mathrm{X}}}{M_{\mathrm{Fe}}} - \log \frac{m_{\mathrm{X}}}{m_{\mathrm{Fe}}}, \quad (3)$$

we can compute the mass of each chemical element, M_{X}, as a function of the mass of gas, M_{g}, out of which these stars have formed. For example, for $M_{\mathrm{g}} \approx 10^{10}\ M_{\odot}$, we get $M_{\mathrm{Fe}} = 9.2 \times 10^{6}\ M_{\odot}$.

By assuming that the following chemical enrichment of the gas, which leads to $A(\mathrm{Fe})^{\mathrm{obs}} = 7.52$ (i.e. [Fe/H]$^{\mathrm{obs}} \approx 0.0$) and $A(\mathrm{Zn}) - A(\mathrm{Fe})]^{\mathrm{obs}} \approx -3.1$, is only driven by SN Ia, we can compute the required mass of SN Ia, M_{SNIa}, along with the final mass of gas, $M_{\mathrm{g}}^{\mathrm{out}}$, by using the following equations:

$$A(\mathrm{Fe})^{\mathrm{obs}} = \log \frac{M_{\mathrm{Fe}} + Y^{\mathrm{Fe_{SNIa}}} \times M_{\mathrm{SNIa}}}{M_{\mathrm{g}}^{\mathrm{out}}} - \log \frac{m_{\mathrm{Fe}}}{m_{\mathrm{H}}} + 12, \quad (4)$$

$$(A(\mathrm{Zn}) - A(\mathrm{Fe}))^{\mathrm{obs}} = \log \frac{M_{\mathrm{Zn}} + Y^{\mathrm{Zn_{SNIa}}} \times M_{\mathrm{SNIa}}}{M_{\mathrm{Fe}} + Y^{\mathrm{Fe_{SNIa}}} \times M_{\mathrm{SNIa}}} - \log \frac{m_{\mathrm{Zn}}}{m_{\mathrm{Fe}}}. \quad (5)$$

We can then exploit the derived M_{SNIa} and $M_{\mathrm{g}}^{\mathrm{out}}$ values to get the expected ("out") alpha-to-iron ratios of several chemical elements. By using the different SN Ia yield models from Iwamoto et al. (1999), and averaging among the corresponding results, we get $(A(\mathrm{Mg}) - A(\mathrm{Fe}))^{\mathrm{out}} = 0.12 \pm 0.002$, $(A(\mathrm{Ca}) - A(\mathrm{Fe}))^{\mathrm{out}} = -1.14 \pm 0.04$ and $(A(\mathrm{S}) - A(\mathrm{Fe}))^{\mathrm{out}} = -0.28 \pm 0.03$[6], which are in good agreement with the observed values at $A(\mathrm{Fe}) = 7.52$, that is, $(A(\mathrm{Ca}) - A(\mathrm{Fe}))^{\mathrm{obs}} = -1.16$, $(A(\mathrm{S}) - A(\mathrm{Fe}))^{\mathrm{obs}} = -0.28$, with the exception of Mg, for which $(A(\mathrm{Mg}) - A(\mathrm{Fe}))^{\mathrm{obs}} = 0.24$ is 0.12 dex higher than the theoretically expected value. Thus, although this picture needs to be carefully tested against other chemical elements and tested exploiting detailed cosmological chemical evolution models, we conclude that it is plausible. Clearly, if the enrichment of SN Ia is really at the origin of the low zinc to iron ratio observed in giant stars located in the inner thin disk, the same trend should be

[6] These findings are independent on the assumed mass of gas, M_{g}.

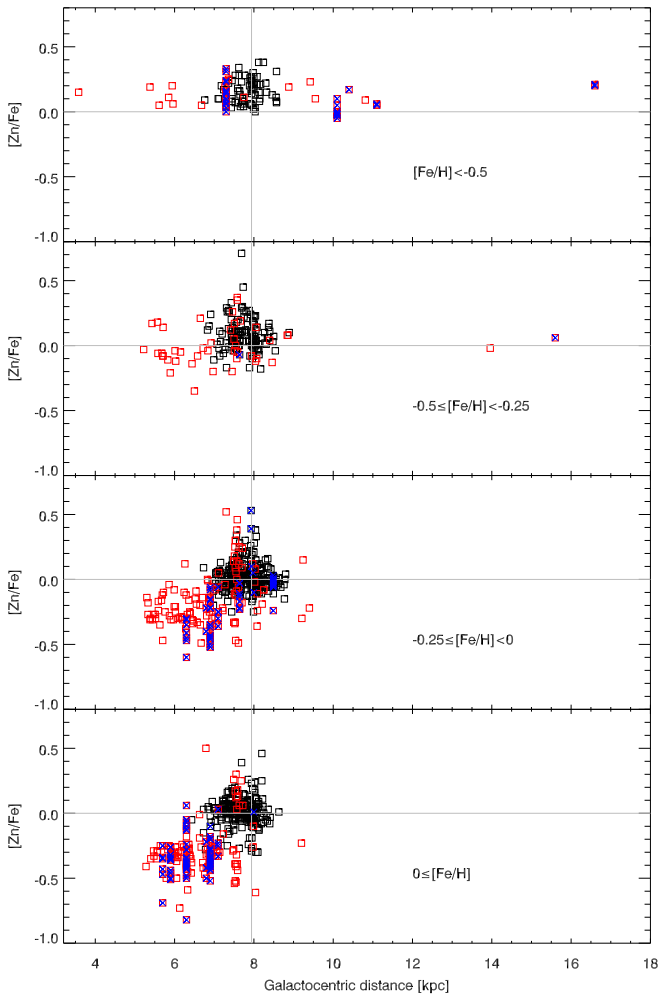

Fig. 16. [Zn/Fe] plotted against R_{GC} for dwarfs (black symbols) and giants (red symbols). Blue crosses indicate stars in clusters. The plot is split to contain only stars in the indicated metallicity range.

observed in dwarf stars, once observed in the same region. Thus, it can in principle be tested observationally, although 30 m-class telescopes will likely be needed.

3.6. Sulphur over zinc

In Fig. 17 the [S/Zn] versus [Zn/H] abundances for the sample of stars analysed for sulphur are shown, by distinguishing among dwarfs, giants and stars in clusters. As already noticed for the [Zn/Fe] versus [Fe/H] trend, we clearly see that dwarfs and giants behave very differently. Dwarf stars show a constant [S/Zn] value (or perhaps a slight slope) around [S/Zn] $\approx$ 0.0 within [Zn/H] $\approx (-0.1, 0.5)$. The slight slope in the dwarf sample might simply be the effect of [S/Fe] increasing more rapidly than [Zn/Fe] as metallicity decreases. On the other hand, giant stars show a declining [S/Zn] trend with [Zn/H], with super-solar [S/Zn] values at [Zn/H] $<$ 0.0 and large scatter. This is due to the giant sample reaching deeper into the inner disk, where the metal rich population shows solar [S/Fe] but subsolar [Zn/Fe].

4. Conclusions

We analysed the sulphur and zinc abundances in a large sample of Galactic stars. Below we summarise our findings for the sample analysed.

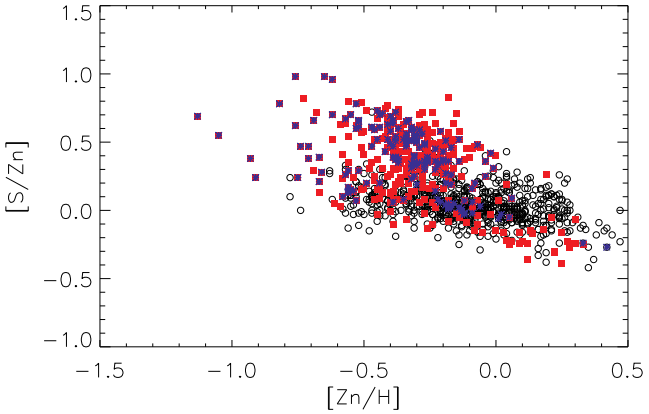

Fig. 17. [S/Zn] vs. [Zn/H] for the sample of GES stars we analysed for sulphur. Symbols are as in Fig. 11.

On sulphur:

- Sulphur behaves as an α-element, with a typical behaviour of [S/Fe] compatible with 0.0 within uncertainties for stars around solar metallicities. The values of [S/Fe] increase for decreasing metallicity with a constant value of [S/Fe] at an [Fe/H] of around −1.0. Unfortunately, due to the weak sulphur feature, the stars in our sample with [Fe/H] ≤ -1.0 are only seven, therefore we cannot make conclusions on the behaviour of sulphur in the metal-poor regime.
- With the line-list we used, we detect a clear trend of [S/Fe] as a function of $T_{\rm eff}$. Further investigations on the contribution of CN molecules in the wavelength range will follow.
- We could not find a cluster with "low" [S/Fe], like Trumpler 5 that, according to Caffau et al. (2014), has a [S/Fe] compatible with Local Group galaxies (Caffau et al. 2005b). All the clusters with [Fe/H] ≤ -0.4 are enhanced in S, as are field stars.
- The open clusters around solar metallicity show, on average, high [S/Fe] values, but we attribute this to the presence of cool stars whose sulphur abundances are systematically "high".
- We confirm and strengthen the detection (Sbordone et al. 2009) of a significant [S/Fe] spread in NGC 104, which appears to correlate to a high degree of significance with [Na/Fe]. While at face value the data appear to show an actual trend of [S/Fe] with [Fe/H], we cannot rule out that we may actually be sampling two different NGC 104 populations, one S-rich and one S-poor, but each without internal sulphur spread.

On zinc:

- In the GES sample, there is a sizeable scatter in the [Zn/Fe] ratios. This scatter is limited to the giant stars around solar metallicity. The giants also appear to be much more concentrated on the thin disk plane.
- At low metallicity ([Fe/H] < -0.5) [Zn/Fe] appears constant at all galactocentic radii, and slightly supersolar.
- As higher metallicities, [Zn/Fe] decreases to the solar value for stars roughly outside $R_{GC} > 7$ kpc.
- Conversely, stars at $R_{GC} < 7$ kpc, despite significant dispersion, show an increasing depletion of Zn with increasing metallicity, down to about [Zn/Fe] $= -0.3$ for stars with [Fe/H] > 0. This behaviour is in agreement with the low [Zn/Fe] values found in the Milky Way Bulge giants by Barbuy et al. (2015).

– The low [Zn/Fe] observed in the (inner) thin disk giants can tentatively be explained as being due to dilution from almost Zn-free SN Ia ejecta, since a compatible level of dilution is observed in Ca and S. However, the observed [Mg/Fe] is 0.12 dex higher than what our simple calculation indicates.

Acknowledgements. We thank the anonymous referee for useful suggestions and comments. The authors are grateful to A. Recio Blanco and P. de Laverny for stimulating discussions regarding the evolution of Zinc in the solar neighbourhood. This work was based on data products from observations made with ESO Telescopes at the La Silla Paranal Observatory under programme ID 188.B-3002. These data products have been processed by the Cambridge Astronomy Survey Unit (CASU) at the Institute of Astronomy, University of Cambridge, and by the FLAMES/UVES reduction team at INAF/Osservatorio Astrofisico di Arcetri. These data have been obtained from the *Gaia*-ESO Survey Data Archive, prepared and hosted by the Wide Field Astronomy Unit, Institute for Astronomy, University of Edinburgh, which is funded by the UK Science and Technology Facilities Council. This work was partly supported by the European Union FP7 programme through ERC grant number 320360 and by the Leverhulme Trust through grant RPG-2012-541. We acknowledge the support from INAF and Ministero dell' Istruzione, dell' Università e della Ricerca (MIUR) in the form of the grant "Premiale VLT 2012 and PRIN-INAF 2014". The results presented here benefit from discussions held during the *Gaia*-ESO workshops and conferences supported by the ESF (European Science Foundation) through the GREAT Research Network Programme. Support for S. D. and L. Sbordone was provided by Chile's Ministry of Economy, Development, and Tourism's Millennium Science Initiative through grant IC120009, awarded to The Millennium Institute of Astrophysics, MAS. The project was funded by FONDATION MERAC. S.S. is supported by the European Commission through a Marie Sklodowska-Curie Fellowship, project PRIMORDIAL, grant agreement: 700907. S.M.A. and S.A.K. acknowledge the SCOPES grant No. IZ73Z0-152485 for financial support. L.M. acknowledges support from "Proyecto interno" #803 of the Universidad Andres Bello. M.T.C. acknowledges the financial support from the Spanish Ministerio de Economía y Competitividad, through grant AYA2013-40611-P. T.B. and S.F. were funded by the project grant "The New Milky Way" from Knut and Alice Wallenberg Foundation. S.G.S. acknowledges the support by Fundação para a Ciência e Tecnologia (FCT) through national funds and a research grant (project ref. UID/FIS/04434/2013, and PTDC/FIS-AST/7073/2014). S.G.S. also acknowledges the support from FCT through Investigador FCT contract of reference IF/00028/2014 and POPH/FSE (EC) by FEDER funding through the program Programa Operacional de Factores de Competitividade – COMPETE. L. Spina acknowledges the support from FAPESP (2014/15706-9). R.S. acknowledges support the Polish Ministry of Science and Higher Education.

References

Allende Prieto, C., Barklem, P. S., Lambert, D. L., & Cunha, K. 2004, A&A, 420, 183
Alvarez, R., & Plez, B. 1998, A&A, 330, 1109
Andrievsky, S. M., Spite, F., Korotin, S. A., et al. 2011, A&A, 530, A10
Babusiaux, C., Katz, D., Hill, V., et al. 2014, A&A, 563, A15
Bagnulo, S., Jehin, E., Ledoux, C., et al. 2003, The Messenger, 114, 10
Bensby, T., Feltzing, S., & Lundström, I. 2003, A&A, 410, 527
Bensby, T., Feltzing, S., Lundström, I., & Ilyin, I. 2005, A&A, 433, 185
Bensby, T., Yee, J. C., Feltzing, S., et al. 2013, A&A, 549, A147
Bensby, T., Feltzing, S., & Oey, M. S. 2014, A&A, 562, A71
Barbuy, B., Friaça, A. C. S., da Silveira, C. R., et al. 2015, A&A, 580, A40
Berg, T. A. M., Ellison, S. L., Prochaska, J. X., Venn, K. A., & Dessauges-Zavadsky, M. 2015, MNRAS, 452, 4326
Bihain, G., Israelian, G., Rebolo, R., Bonifacio, P., & Molaro, P. 2004, A&A, 423, 777
Bonifacio, P., Spite, M., Cayrel, R., et al. 2009, A&A, 501, 519
Bonifacio, P., Caffau, E., Venn, K. A., & Lambert, D. L. 2012, A&A, 544, A102
Bragaglia, A., & Tosi, M. 2006, AJ, 131, 1544
Bressan, A., Marigo, P., Girardi, L., et al. 2012, MNRAS, 427, 127
Caffau, E., & Ludwig, H.-G. 2007, A&A, 467, L11
Caffau, E., Bonifacio, P., Faraggiana, R., et al. 2005a, A&A, 441, 533
Caffau, E., Bonifacio, P., Faraggiana, R., & Sbordone, L. 2005b, A&A, 436, L9
Caffau, E., Faraggiana, R., Bonifacio, P., Ludwig, H.-G., & Steffen, M. 2007, A&A, 470, 699
Caffau, E., Sbordone, L., Ludwig, H.-G., Bonifacio, P., & Spite, M. 2010, Astron. Nachr., 331, 725
Caffau, E., Ludwig, H.-G., Steffen, M., Freytag, B., & Bonifacio, P. 2011, Sol. Phys., 268, 2, 255
Caffau, E., Monaco, L., Spite, M., et al. 2014, A&A, 568, A29
Caffau, E., Andrievsky, S., Korotin, S., et al. 2016, A&A, 585, A16
Calura, F., & Menci, N. 2009, MNRAS, 400, 1347
Calura, F., Dessauges-Zavadski, M., Prochaska, J. X., & Matteucci, F. 2009, ApJ, 693, 1236
Carraro, G., Geisler, D., Villanova, S., Frinchaboy, P. M., & Majewski, S. R. 2007, A&A, 476, 217
Castelli, F., & Kurucz, R. L. 2003, Modelling of Stellar Atmospheres, 210, A20
Cayrel, R. 1988, in The Impact of Very High S/N Spectroscopy on Stellar Physics, IAU Symp., 132, 345
Cayrel, R., Depagne, E., Spite, M., et al. 2004, A&A, 416, 1117
Centurión, M., Bonifacio, P., Molaro, P., & Vladilo, G. 2000, ApJ, 536, 540
Chabrier, G. 2001, ApJ, 554, 1274
Chen, Y. Q., Nissen, P. E., Benoni, T., & Zhao, G. 2001, A&A, 371, 943
Chen, Y. Q., Nissen, P. E., Zhao, G., & Asplund, M. 2002, A&A, 390, 225
Chen, Y. Q., Zhao, G., Nissen, P. E., Bai, G. S., & Qiu, H. M. 2003, ApJ, 591, 925
Chiappini, C., Matteucci, F., Beers, T. C., & Nomoto, K. 1999, ApJ, 515, 226
Chieffi, A., & Limongi, M. 2004, ApJ, 608, 405
Clegg, R. E. S., Tomkin, J., & Lambert, D. L. 1981, ApJ, 250, 262
Cordero, M. J., Pilachowski, C. A., Johnson, C. I., et al. 2014, ApJ, 780, 94
Dekker, H., D'Odorico, S., Kaufer, A., Delabre, B., & Kotzlowski, H. 2000, Proc. SPIE, 4008, 534
Dobrovolskas, V., Kučinskas, A., Bonifacio, P., et al. 2014, A&A, 565, A121
Ecuvillon, A., Israelian, G., Santos, N. C., Mayor, M., Villar, V., & Bihain, G. 2004, A&A, 426, 619
Eisenhauer, F., Schödel, R., Genzel, R., et al. 2003, ApJ, 597, L121
Fitzpatrick, E. L., & Massa, D. 2007, ApJ, 663, 320
François, P. 1987, A&A, 176, 294
François, P. 1988, A&A, 195, 226
Frebel, A., Aoki, W., Chistlieb, N., et al. 2005, IAU Symp. Proc., 228, 207
Frebel, A., Simon, J. D., Geha, M., & Willman, B. 2010, ApJ, 708, 560
Frebel, A., Simon, J. D., & Kirby, E. N. 2014, ApJ, 786, 74
Frebel, A., Norris, J. E., Gilmore, G., & Wyse, R. F. G. 2016, ApJ, 826, 110
Fuhrmann, K. 1998, A&A, 338, 161
Fuhrmann, K. 1999, Ap&SS, 265, 265
Fuhrmann, K. 2004, Astron. Nachr., 325, 3
Garnett, D. R. 1989, ApJ, 345, 282
Greggio, L., & Renzini, A. 1983, A&A, 118, 217
Gilmore, G., Randich, S., Asplund, M., et al. 2012, The Messenger, 147, 25
Harris, W. E. 1996, AJ, 112, 1487
Hayden, M. R., Bovy, J., Holtzman, J. A., et al. 2015, ApJ, 808, 132
Haywood, M., Lehnert, M. D., Di Matteo, P., et al. 2016, A&A, 589, A66
Hoffman, R. D., Woosley, S. E., Fuller, G. M., & Meyer, B. S. 1996, ApJ, 460, 478
Holtzman, J. A., Shetrone, M., Johnson, J. A., et al. 2015, AJ, 150, 148
Ishigaki, M. N., Aoki, W., & Chiba, M. 2013, ApJ, 771, 67
Israelian, G., & Rebolo, R. 2001, ApJ, 557, L43
Iwamoto, K., Brachwitz, F., Nomoto, K., et al. 1999, ApJS, 125, 439
Jacobson, H. R., Friel, E. D., Jílková, L., et al. 2016, A&A, 591, A37
Jenkins, E. B. 2009, ApJ, 700, 1299
Ji, A. P., Frebel, A., Simon, J. D., & Chiti, A. 2016, ApJ, 830, 93
Johnson, C. I., McDonald, I., Pilachowski, C. A., et al. 2015, AJ, 149, 71
Jönsson, H., Ryde, N., Nissen, P. E., et al. 2011, A&A, 530, A144
Kacharov, N., Koch, A., Caffau, E., & Sbordone, L. 2015, A&A, 577, A18
Käufl, H.-U., Ballester, P., Biereichel, P., et al. 2004, in Ground-based Instrumentation for Astronomy, eds. A. F. M. Moorwood, & I. Masanori, Proc. SPIE, 5492, 1218
Kobayashi, C., Umeda, H., Nomoto, K., Tominaga, N., & Ohkubo, T. 2006, ApJ, 653, 1145
Koch, A., & Caffau, E. 2011, A&A, 534, A52
Korn, A. J., & Ryde, N. 2005, A&A, 443, 1029
Korotin, S. A. 2008, Odessa Astronomical Publications, 21, 42
Korotin, S. A. 2009, Astron. Rep., 53, 651
Limongi, M., & Chieffi, A. 2003, ApJ, 592, 404
Lind, K., Bergemann, M., & Asplund, M. 2012, MNRAS, 427, 50
Lodders, K., Palme, H., & Gail, H.-P. 2009, Landolt-Börnstein – Group VI Astronomy and Astrophysics Numerical Data and Functional Relationships in Science and Technology Volume, 4, 44
Ludwig, H.-G., Caffau, E., Steffen, M., et al. 2009, Mem. Soc. Astron. Ital., 80, 711
Mannucci, F., Della Valle, M., & Panagia, N. 2006, MNRAS, 370, 773
Marino, A. F., Milone, A. P., Casagrande, L., et al. 2016, MNRAS, 459, 610
Mashonkina, L., Gehren, T., Shi, J.-R., et al. 2011, A&A, 528, A87
Matrozis, E., Ryde, N., & Dupree, A. K. 2013, A&A, 559, A115
Matteucci, F., & Brocato, E. 1990, ApJ, 365, 539
McLaughlin, D. E., & van der Marel, R. P. 2005, ApJS, 161, 304
McWilliam, A. 2016, PASA, 33, e040
Mikolaitis, Š., Hill, V., Recio-Blanco, A., et al. 2014, A&A, 572, A33
Mishenina, T. V., Kovtyukh, V. V., Soubiran, C., Travaglio, C., & Busso, M. 2002, A&A, 396, 189

Moore, C. E. 1945, Contributions from the Princeton University Observatory, 20, 1
Montgomery, K. A., Marschall, L. A., & Janes, K. A. 1993, AJ, 106, 181
Nidever, D. L., Bovy, J., Bird, J. C., et al. 2014, ApJ, 796, 38
Nissen, P. E. 2015, A&A, 579, A52
Nissen, P. E., & Schuster, W. J. 2011, A&A, 530, A15
Nissen, P. E., Chen, Y. Q., Asplund, M., & Pettini, M. 2004, A&A, 415, 993
Nissen, P. E., Akerman, C., Asplund, M., et al. 2007, A&A, 469, 319
Nomoto, K., Thielemann, F.-K., & Wheeler, J. C. 1984, ApJ, 279, L23
Nomoto, K., Hashimoto, M., Tsujimoto, T., et al. 1997a, Nucl. Phys. A, 616, 79
Nomoto, K., Iwamoto, K., Nakasato, N., et al. 1997b, Nucl. Phys. A, 621, 467
Pancino, E., Lardo, C., Altavilla, G., et al. (Gaia Collaboration) 2017, A&A, 598, A5
Pasquini, L., Avila, G., Blecha, A., et al. 2002, The Messenger, 110, 1
Piskunov, A. E., Schilbach, E., Kharchenko, N. V., Röser, S., & Scholz, R.-D. 2008, A&A, 477, 165
Plez, B. 2012, Astrophysics Source Code Library [record ascl:1205.004]
Pompéia, L. 2003, Astrophys. Space Sci. Lib., 299
Primas, F., Brugamyer, E., Sneden, C., et al. 2000, Liege International Astrophysical Colloquia, 35, 119
Prochaska, J. X., Naumov, S. O., Carney, B. W., McWilliam, A., & Wolfe, A. M. 2000, AJ, 120, 2513
Gaia Collaboration (Prusti, T., et al.) 2016, A&A, 595, A1
Randich, S., Gilmore, G., & Gaia-ESO Consortium 2013, The Messenger, 154, 47
Recio-Blanco, A., de Laverny, P., Kordopatis, G., et al. 2014, A&A, 567, A5
Reddy, B. E., Tomkin, J., Lambert, D. L., & Allende Prieto, C. 2003, MNRAS, 340, 304
Reddy, B. E., Lambert, D. L., & Allende Prieto, C. 2006, MNRAS, 367, 1329
Roederer, I. U., Placco, V. M., & Beers, T. C. 2016, ApJ, 824, L19
Ryde, N. 2006, A&A, 455, L13
Ryde, N., & Lambert, D. L. 2004, A&A, 415, 559
Ryde, N., Jönsson, H., & Matrozis, E. 2014, Mem. Soc. Astron. Ital., 85, 269
Sacco, G. G., Morbidelli, L., Franciosini, E., et al. 2014, A&A, 565, A113
Savage, B. D., & Sembach, K. R. 1996, ARA&A, 34, 279
Sbordone, L., Bonifacio, P., Buonanno, R., et al. 2007, A&A, 465, 815
Sbordone, L., Limongi, M., Chieffi, A., et al. 2009, A&A, 503, 121
Sbordone, L., Caffau, E., Bonifacio, P., & Duffau, S. 2014, A&A, 564, A109
Skúladóttir, Á., Andrievsky, S. M., Tolstoy, E., et al. 2015, A&A, 580, A129
Smiljanic, R., Korn, A. J., Bergemann, M., et al. 2014, A&A, 570, A122
Sneden, C., & Crocker, D. A. 1988, ApJ, 335, 406
Sneden, C., Gratton, R. G., & Crocker, D. A. 1991, A&A, 246, 354
Spina, L., Meléndez, J., Karakas, A. I., et al. 2016, A&A, 593, A125
Spina, L., Randich, S., Magrini, L., et al. 2017, A&A, 601, A70
Spite, M., et al. 2011, A&A, 528, A9
Stonkutė, E., Koposov, S. E., Howes, L. M., et al. 2016, MNRAS, 460, 1131
Takada-Hidai, M., & Takeda, Y. 1996, PASJ, 48, 739
Takada-Hidai, M., Takeda, Y., Sato, S., et al. 2002, ApJ, 573, 614
Takeda, Y., & Takada-Hidai, M. 2011, PASJ, 63, 537
Takeda, Y., & Takada-Hidai, M. 2012, PASJ, 64, 42
Takeda, Y., Hashimoto, O., Taguchi, H., et al. 2005, PASJ, 57, 751
Takeda, Y., Omiya, M., Harakawa, H., & Sato, B. 2016, PASJ, 68, 81
Thygesen, A. O., Sbordone, L., Andrievsky, S., et al. 2014, A&A, 572, A108
Tinsley, B. M. 1979, ApJ, 229, 1046
Tolstoy, E., Hill, V., & Tosi, M. 2009, ARA&A, 47, 371
Travaglio, C., Gallino, R., Arnone, E., et al. 2004, ApJ, 601, 864
VandenBerg, D. A., Brogaard, K., Leaman, R., & Casagrande, L. 2013, ApJ, 775, 134
Venn, K. A., Irwin, M., Shetrone, M. D., et al. 2004, AJ, 128, 1177
Venn, K. A., Shetrone, M. D., Irwin, M. J., et al. 2012, ApJ, 751, 102
Wallerstein, G., & Conti, P. 1964, ApJ, 140, 858
Wojno, J., Kordopatis, G., Steinmetz, M., et al. 2016, MNRAS, 461, 4246
Wolfe, A. M., Gawiser, E., & Prochaska, J. X. 2005, ARA&A, 43, 861
Woosley, S. E., & Weaver, T. A. 1995, ApJS, 101, 181

[1] Millennium Institute of Astrophysics, 1515 Santiago, Chile
e-mail: sonia.duffau@gmail.com
[2] Instituto de Astrofísica, Pontificia Universidad Católica de Chile, Av. Vicuña Mackenna 4860, 782-0436 Macul, Santiago, Chile
[3] Departamento de Ciencias Fisicas, Universidad Andres Bello, Fernandez Concha 700, Las Condes, Santiago, Chile
[4] GEPI, Observatoire de Paris, PSL Research University, CNRS, Place Jules Janssen, 92195 Meudon, France
[5] European Southern Observatory, Alonso de Cordova 3107, Vitacura, Santiago de Chile, Chile
[6] Department of Astronomy and Astronomical Observatory, Odessa National University, Isaac Newton Institute of Chile, Odessa Branch, Shevchenko Park, 65014 Odessa, Ukraine
[7] Crimean Astrophysical Observatory, 298409 Nauchny, Crimea
[8] UPJV, Université de Picardie Jules Verne, 33 rue St Leu, 80080 Amiens, France
[9] Kapteyn Astronomical Institute, University of Groningen, Landleven 12, 9747 AD Groningen, The Netherlands
[10] Max-Planck-Institut für Astronomie, Königstuhl 17, 69117 Heidelberg, Germany
[11] INAF–Osservatorio Astronomico di Bologna, via Gobetti 93/3, 40129 Bologna, Italy
[12] Dipartimento di Astronomia, Universitá di Bologna, via Gobetti 93/2, 40129 Bologna, Italy
[13] Universidade de Sao Paulo, IAG, Departamento de Astronomia, Rua do Matao 1226, 05509-900 Sao Paulo, SP, Brasil
[14] Zentrum für Astronomie der Universität Heidelberg, Landessternwarte, Königstuhl 12, 69117 Heidelberg, Germany
[15] Technische Universität Darmstadt, Schlossgartenstr. 2, 64289 Darmstadt, Germany
[16] Dark Cosmology Centre, The Niels Bohr Institute, Juliane Maries Vej 30, 2100 Copenhagen, Denmark
e-mail: cjhansen@dark-cosmology.dk
[17] Leibniz-Institut für Astrophysik Potsdam, An der Sternwarte 16, 14482 Potsdam, Germany
[18] Istituto Nazionale di Astrofisica, Osservatorio Astronomico di Padova Vicolo dell'Osservatorio 5, 35122 Padova, Italy
[19] Observatoire de Genève, Université de Genève, C1290 Versoix, Switzerland
[20] Department of Astronomy, Indiana University, 727 East 3rd St, Swain West 318, Bloomington, IN 47405, USA
[21] Centro de Astrobiología (INTA-CSIC), Departamento de Astrofísica, PO Box 78, 28691 Villanueva de la Cañada, Madrid, Spain
[22] Phyics Department, Lancaster University, Lancaster LA1 4YB, UK
[23] INAF–Osservatorio Astrofisico di Arcetri, Largo E. Fermi 5, 50125, Florence, Italy
[24] ASI Science Data Center, Via del Politecnico SNC, 00133 Roma, Italy
[25] Departamento de Astronomía, Casilla 160-C, Universidad de Concepción, Chile
[26] Institute of Theoretical Physics and Astronomy, Vilnius University, Sauletekio av. 3, 10222 Vilnius, Lithuania
[27] Department of Astronomy, Columbia University, 550 W 120th St, New York, NY 10027, USA
[28] Institute of Astronomy, University of Cambridge, Madingley Road, Cambridge CB3 0HA, UK
[29] Lund Observatory, Department of Astronomy and Theoretical Physics, Box 43, 221 00 Lund, Sweden
[30] Nicolaus Copernicus Astronomical Center, Polish Academy of Sciences, ul. Bartycka 18, 00-716 Warsaw, Poland
[31] Instituto de Física y Astronomía, Universidad de Valparaíso, 951 Valparaíso, Chile
[32] Dipartimento di Fisica e Astronomia, Universitá di Padova, Vicolo Osservatorio 3, 35122 Padova, Italy
[33] Instituto de Astrofísica de Andalucía-CSIC, Apdo. 3004, 18080 Granada, Spain
[34] INAF–Osservatorio Astronomico di Palermo, Piazza del Parlamento 1, 90134 Palermo, Italy
[35] Núcleo de Astronomía, Facultad de Ingeniería, Universidad Diego Portales, Av. Ejercito 441, Santiago, Chile
[36] Laboratoire d'astrophysique, Ecole Polytechnique Fédérale de Lausanne (EPFL), Observatoire de Sauverny, 1290 Versoix, Switzerland
[37] Instituto de Astrofísica e Ciências do Espaço, Universidade do Porto, CAUP, Rua das Estrelas, 4150-762 Porto, Portugal